GLACIERS

Glacier preservation doubled by limiting warming to 1.5°C versus 2.7°C

Harry Zekollari[1,2,3]*†, Lilian Schuster[4]*†, Fabien Maussion[5], Regine Hock[6,7], Ben Marzeion[8,9], David R. Rounce[10], Loris Compagno[2,11,12], Koji Fujita[13], Matthias Huss[2,11,14], Megan James[15], Philip D. A. Kraaijenbrink[16], William H. Lipscomb[17], Samar Minallah[17], Moritz Oberrauch[18,19], Lander Van Tricht[2,11,1], Nicolas Champollion[20], Tamsin Edwards[15], Daniel Farinotti[2,11], Walter Immerzeel[16], Gunter Leguy[17], Akiko Sakai[13]

Glaciers adapt slowly to changing climatic conditions, with long-term implications for sea-level rise and water supply. Using eight glacier models, we simulated global glacier evolution over multicentennial timescales, allowing glaciers to equilibrate with climate under various constant global temperature scenarios. We estimate that glaciers globally will lose 39 (range, 15 to 55)% of their mass relative to 2020, corresponding to a global mean sea-level rise of 113 (range, 43 to 204) mm even if temperatures stabilized at present-day conditions. Under the +1.5°C Paris Agreement goal, more than twice as much global glacier mass remains at equilibration (53% versus 24%) compared with the warming level resulting from current policies (+2.7°C by 2100 above preindustrial). Our findings stress the need for stringent mitigation policies to ensure the long-term preservation of glaciers.

Global-scale glacier mass loss profoundly affects our society and the natural environment, contributing to sea-level rise (*1*–*3*), influencing downstream water resources (*4*), affecting biodiversity and ecosystems (*5*), exacerbating natural hazards (*6*), and having a negative effect on the tourism industry (*7*). Recent projections of all glaciers outside of the Antarctic and Greenland ice sheets, based on a range of transient climate scenarios, estimate mass losses of ~20 to 50% between 2015 and 2100 depending on emissions scenarios (*8*–*11*). However, even if the current climate were to stabilize, then glaciers would be expected to continue losing mass over extended time periods (*12*–*14*). Glaciers may vanish entirely or, if the new climatic conditions permit, retreat until they reach a steady state in which glacier mass and glacier geometry remain approximately stable (*15*). This continued loss after climate stabilization is due to the slow adjustment of a glacier's geometry, driven by the gradual flow of ice from high to low elevations (*16*, *17*). Additionally, the lag between the climatic forcing and glacier response is influenced by feedback mechanisms involving elevation and mass balance (*18*), as well as albedo and mass balance (*19*).

Observational and modeling studies suggest that the time needed for glaciers to reach a new steady state after a climate perturbation can range from decades to multiple centuries (*20*–*22*). However, the mass losses that are committed but not yet realized in response to long-term climate stabilization remain largely unquantified, with insights primarily derived from only two exploratory studies. Mernild *et al.* (*23*) used observed ratios of accumulation to total glacier area to estimate present-day committed global mass losses, and Marzeion *et al.* (*13*) used a glacier evolution model based on volume-area scaling to project committed losses across various global mean temperature scenarios. Both studies agree on the estimate that ~35 to 40% of glacier mass will be lost under early 21st-century climatic conditions. However, Marzeion *et al.* (*13*) did not account for glaciers in the Greenland Periphery and the Subantarctic & Antarctic Islands. Moreover, both studies relied on limited observations to constrain and evaluate their methods, possibly affecting the precision and reliability of their methods and conclusions.

Here, we used eight state-of-the-art glacier evolution models to simulate long-term glacier mass loss of all glaciers outside of the ice sheets for 80 constant-climate scenarios. These constant-climate scenarios were derived by repeating eight different 20-year periods between 1850 and 2100 from various climate models forced by Shared Socioeconomic Pathways (fig. S1 and materials and methods). Our diverse scenarios form an ensemble of global and regional climates, each of which is associated with a change in global mean temperature compared with preindustrial. The glacier models are run for several thousand years to ensure that the glaciers have sufficient time to equilibrate with the new climate. These long-term simulations thus enable the quantification of the committed glacier mass loss at regional and global scales under diverse policy-relevant global warming levels.

Committed glacier mass changes under present-day climate

Our model simulations project that if current (2014 to 2023) climatic conditions [global mean temperature change (ΔT) = 1.2°C above preindustrial (*24*)] were to persist, glaciers would eventually lose 39% (range, 15 to 55%) of their global glacier mass relative to 2020 [the 17th to 83rd percentiles are the International Panel on Climate Change's (*25*) "likely range"; Fig. 1 and table S1]. This already committed, but not yet fully realized, glacier mass loss is projected to contribute 113 mm (range, 43 to 204 mm) to global mean sea-level rise, irrespective of any future warming. This substantial present-day committed mass loss highlights that today's glaciers are strongly out of balance with current climatic conditions due to their long response times. The strong imbalance between glacier geometry and climate is exacerbated by atmospheric warming being particularly pronounced at high elevations (*26*) and high latitudes (*27*) where glaciers are predominantly located. In our ensemble of climate models, the median air temperature increase over glacier areas is 80% higher than the global average, a relationship that is consistent regardless of the future global temperature increase (fig. S2 and materials and methods).

The imbalance between current climate and glacier geometry varies greatly among regions, resulting in sharply contrasting regional present-day committed losses (Figs. 2 and 3 and table S1). Relative losses of some regions are small, such as South Asia West [5% (range, 0 to 30%) under ΔT = 1.2°C], Central Asia [12% (range, 3 to 32%)], and New Zealand [15% (range, 2 to 39%)], whereas other regions are projected to experience substantial losses regardless of further future warming, such as Arctic Canada South [85% (range, 83 to 94%)], Western Canada & US [74% (range, 43 to 93%)], Scandinavia [66% (range, 24 to 85%)], and Russian Arctic [65% (range, 46 to 80%)].

[1]Department of Water and Climate, Vrije Universiteit Brussel, Brussels, Belgium. [2]Laboratory of Hydraulics, Hydrology and Glaciology (VAW), ETH Zürich, Zürich, Switzerland. [3]Laboratoire de Glaciologie, Université libre de Bruxelles, Brussels, Belgium. [4]Department of Atmospheric and Cryospheric Sciences (ACINN), Universität Innsbruck, Innsbruck, Austria. [5]Bristol Glaciology Centre, School of Geographical Sciences, University of Bristol, Bristol, UK. [6]Department of Geosciences, University of Oslo, Oslo, Norway. [7]Geophysical Institute, University of Alaska Fairbanks, Fairbanks, AK, USA. [8]Institute of Geography, University of Bremen, Bremen, Germany. [9]MARUM - Center for Marine Environmental Sciences, University of Bremen, Bremen, Germany. [10]Department of Civil and Environmental Engineering, Carnegie Mellon University, Pittsburgh, PA, USA. [11]Swiss Federal Institute for Forest, Snow and Landscape Research (WSL), bâtiment ALPOLE, Sion, Switzerland. [12]Swiss Reinsurance Company Ltd (Swiss Re), Zürich, Switzerland. [13]Graduate School of Environmental Studies, Nagoya University, Nagoya, Japan. [14]Department of Geosciences, University of Fribourg, Fribourg, Switzerland. [15]Department of Geography, King's College London, London, UK. [16]Department of Physical Geography, Utrecht University, Utrecht, Netherlands. [17]NSF National Center for Atmospheric Research, Boulder, CO, USA. [18]WSL-Institute for Snow and Avalanche Research SLF, Davos, Switzerland. [19]Department of Civil, Environmental and Geomatic Engineering, ETH Zürich, Zürich, Switzerland. [20]Institut des Géosciences de l'Environnement (IGE), Université Grenoble Alpes, Grenoble, France. ***Corresponding author. Email: harry.zekollari@vub.be (H.Z.); lilian.schuster@uibk.ac.at (L.S.)** †These authors contributed equally to this work.

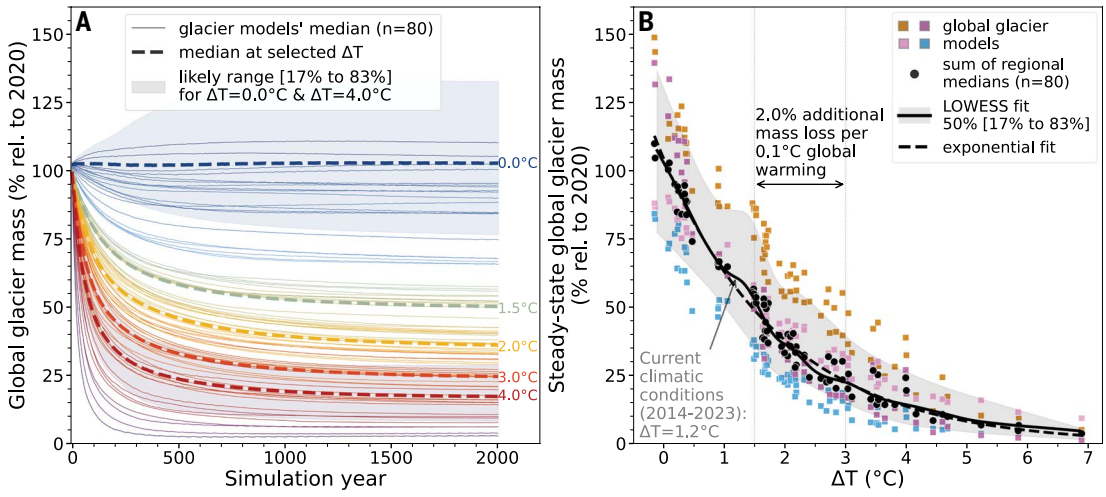

Fig. 1. Projected global glacier mass under constant-climate scenarios. (**A**) Evolution of global glacier mass relative to present day (year 2020; 3-year running mean). Solid lines show the results for all 80 constant-climate scenarios derived from the sum of the regional medians of the glacier model ensemble. Colors indicate corresponding global mean warming levels above preindustrial (ΔT, range from −0.1° to 6.9°C). Dashed lines refer to the mean of the solid lines for select warming levels. Shading marks the multimodel ensemble likely range (shown for $\Delta T = 0.0 \pm 0.2$°C and $\Delta T = 4.0 \pm 0.2$°C). (**B**) Steady-state glacier mass as a function of warming level. Colored dots refer to results for the globally applied glacier models (color coding per glacier model is in Fig. 2). Black dots are obtained by globally summing regional multimodel medians through which a LOWESS fit is added.

These regional differences in relative present-day committed losses are correlated with regional glacier elevation range (the highest correlation among the variables considered, $r = -0.55$; fig. S3 and Fig. 4A). Regions where glaciers span a wide elevation range, typically located at lower latitudes with rugged mountain topography, have a higher potential to adapt to changing climatic conditions, because glaciers can (partly) survive by retreating to higher elevations. Conversely, regions with smaller glacier elevation ranges tend to have higher present-day committed losses. In these regions, glaciers have less potential to retreat to higher elevations, an effect that is particularly pronounced in Arctic Canada South (Fig. 4A). Combined with strong regional warming (2.2 times the global warming; Fig. 2 and fig. S4), Canada South's glaciers are projected to largely disappear in the coming centuries under present-day climatic conditions. Many of this region's large glaciers are relics of past glaciations [e.g., the 6000 km^2 Barnes ice cap, a remnant of the Laurentide ice sheet (*28*, *29*)] and cannot survive.

Committed glacier mass changes under policy-relevant scenarios

If global temperatures stabilize at the limits targeted in the Paris Agreement, then glaciers are projected to eventually lose 47% (range, 20 to 64%) of their global mass relative to 2020 for a +1.5°C scenario and 63% (range, 43 to 76%) for a +2.0°C scenario, contributing 138 mm (range, 59 to 237 mm) and 190 mm (range, 128 to 279 mm) to global mean sea-level rise, respectively (all values at steady state). Under current climate policy pledges, global temperatures are projected to reach 2.7°C above preindustrial levels by 2100 (*30*), which would result in eventually losing 76% (range, 54 to 82%) of glacier mass globally, corresponding to 230 mm (range, 159 to 302 mm) of sea-level rise. Thus, more than twice as much global glacier mass is projected to remain long term under the Paris Agreement +1.5°C goal compared with current climate policies.

Every additional 0.1°C increase between the +1.5°C and +3.0°C scenario eventually results in an additional 2.0% (range, 1.6 to 2.4%) global glacier mass loss, corresponding to 6.5 mm (range, 4.6 to 8.9 mm) of sea-level rise from glaciers alone (Fig. 1B and table S1). Considering the same domain (i.e., without the Subantarctic & Antarctic Islands and the Greenland Periphery), our sensitivity derived from eight glacier models is consistent with that by Marzeion *et al.* (*13*), which was based on a single model (fig. S7). For context, recent glacier projections performed with PyGEM-OGGM (*10*) estimated that a +3.0°C scenario would result in ~8% more global glacier mass loss by 2100 relative to 2015 (34-mm sea-level rise) than the +1.5°C scenario. In their simulations, every 0.1°C increase leads to an additional ~0.6% mass loss and 2.3-mm sea-level rise over the period 2015 to 2100. The glacier mass loss sensitivity to temperature increase revealed by our experiments based on long-term equilibrated glacier masses is three times larger (2.0% per 0.1°C) when considering all models, or about two times larger (1.4% per 0.1°C) when considering PyGEM-OGGM alone (fig. S5), indicating that substantial mass losses resulting from current climate policies will manifest after 2100.

The committed mass loss sensitivity to climate policies varies considerably across regions. Regions currently closest to balance with their climatic conditions, i.e., those with the smallest committed loss under present-day conditions, are the most sensitive to future warming (Fig. 4B and table S1). These regions include South Asia West [3.4% (range, 2.0 to 3.6%) per +0.1°C for $\Delta T = 1.5$ to 3.0°C], Central Asia [3.0% (range, 2.2 to 3.2%) per +0.1°C], the Low Latitudes [3.0% (range, 2.1 to 3.7%) per +0.1°C], and New Zealand [2.9% (range, 2.7 to 2.9%) per +0.1°C]. Therefore, although these regions are projected to experience less relative mass loss under present-day climatic conditions than others, they will be the most affected by future warming levels from current climate policies.

At higher warming levels, the relation between committed global glacier losses and warming levels becomes nonlinear. At +3.0°C, glaciers are projected to lose 77% (range, 60 to 85%) of their global mass, with all 19 regions losing more than two-thirds of their present-day mass and nine of those regions losing more than 90% (table S1). Consequently, in many regions, additional warming above +3.0°C leads to less additional glacier mass loss, because there is little mass left to lose, thereby reducing the sensitivity of global glacier mass loss to temperature change (Fig. 1B). In a 4°C warmer world, glaciers are projected to lose 86% (range, 74 to 93%) of their present-day mass globally, with most midlatitude regions deglaciating (<5% of mass remaining). In an extreme 5°C warmer world corresponding to the upper range of warming projected by 2100 under SSP5-8.5, 91% (range, 82 to 96%) of global glacier mass is lost in the long term, contributing about 282 mm (range, 242 to 352 mm) to sea-level rise.

Conversely, preserving the present-day global glacier mass would require a return to preindustrial temperatures (1850 to 1900; $\Delta T = +0.0$°C; Fig. 1A). Glaciers were substantially larger than today in the second half of the 19th century due to colder and/or wetter climatic conditions in the 18th and early 19th centuries (*22*, *31*–*33*). The retreat of glaciers in the early 20th century was a response to this imbalance, which has more recently been amplified and overtaken by human-induced warming (*34*, *35*). Without anthropogenic warming, present-day temperatures would be close to preindustrial levels (*25*), and glaciers would be larger than they are now. In this hypothetical case, global glacier mass would today still be declining toward the present-day observed glacier mass, a multicentennial process.

Climate policies and multicentennial glacier evolution: a tale of contrasting timescales

Approximately a millennium is needed for the global glacier mass to fully respond and equilibrate with the most optimistic warming level

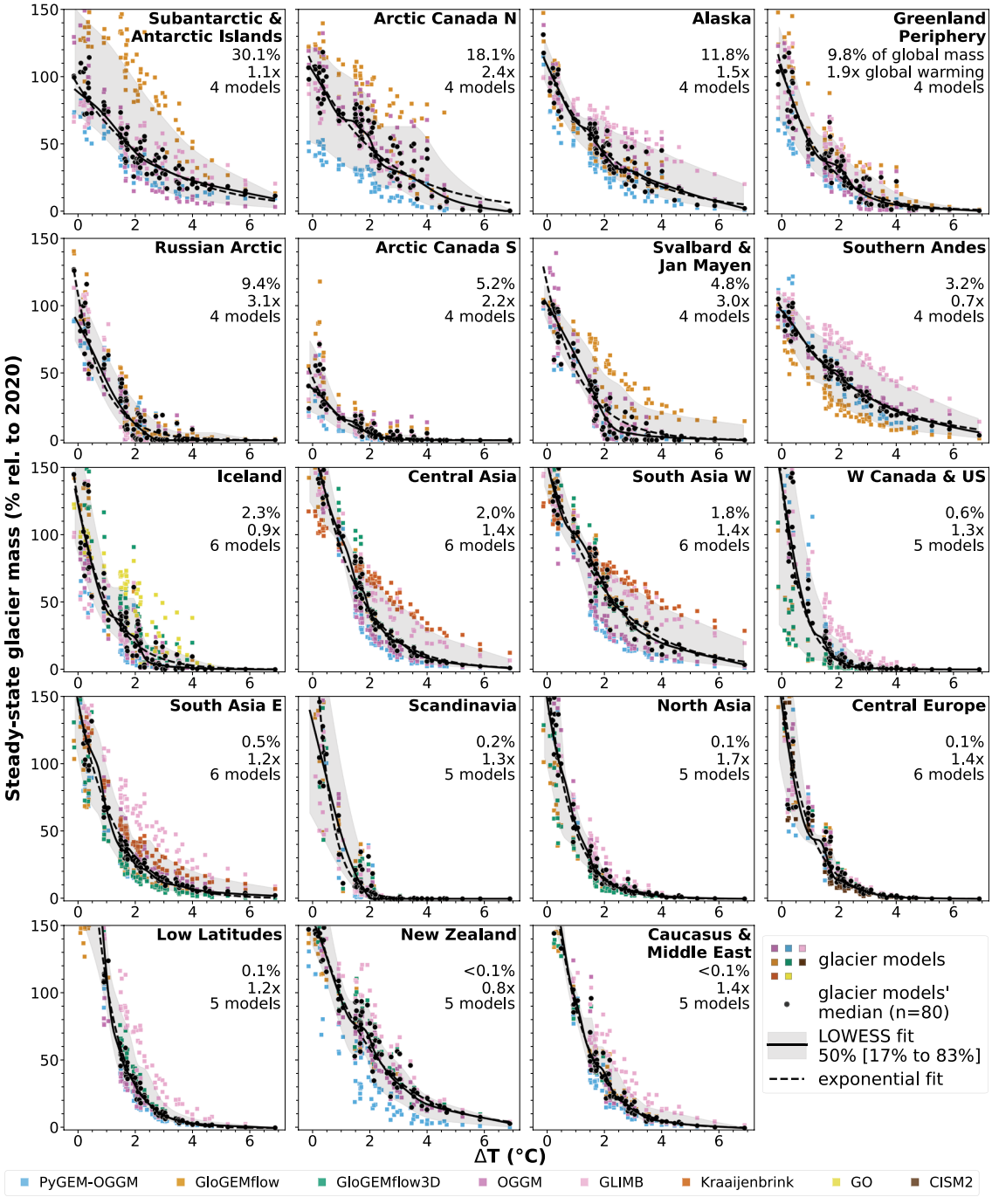

Fig. 2. Regional steady-state glacier masses relative to present day (year 2020) as a function of global warming levels above preindustrial (ΔT). Dots represent individual simulations forced by 80 constant-climate scenarios per glacier model (four to six glacier models per region, color coded). Regions are sorted by descending present-day (2020) glacier mass. For each region, the percentage of global glacier mass in 2020, the warming over the glacierized area relative to the global mean warming (versus 1986 to 2005, median value over 80 climate scenarios; see the materials and methods), and the number of glacier models used are given. For fits with respect to warming levels over each region's glacierized area, see fig. S4; for individual glacier models, see fig. S5; and for regional masses after 100 years, see fig. S6.

outlined in the Paris Agreement (ΔT = +1.5°C; Fig. 1A and fig. S8). This long response time is largely due to high-latitude regions, which contain by far most of the global glacier mass and require multicentury timescales to respond to changing climatic conditions. Most notably, the Subantarctic & Antarctic Islands require more than 800 years for 80% of committed mass loss to occur for a +1.5°C scenario (Fig. 4, C and D). Other regions, such as the Arctic Canada North, Russian Arctic, Greenland Periphery, Iceland, Svalbard, and Arctic Canada South, also respond on long timescales, with 80% changes taking more than 200 years (table S1). These slow-responding regions are characterized by gently sloping glaciers (Fig. 4C and fig. S3), contrasting with regions with steeper glaciers, where most changes occur within a few decades, such

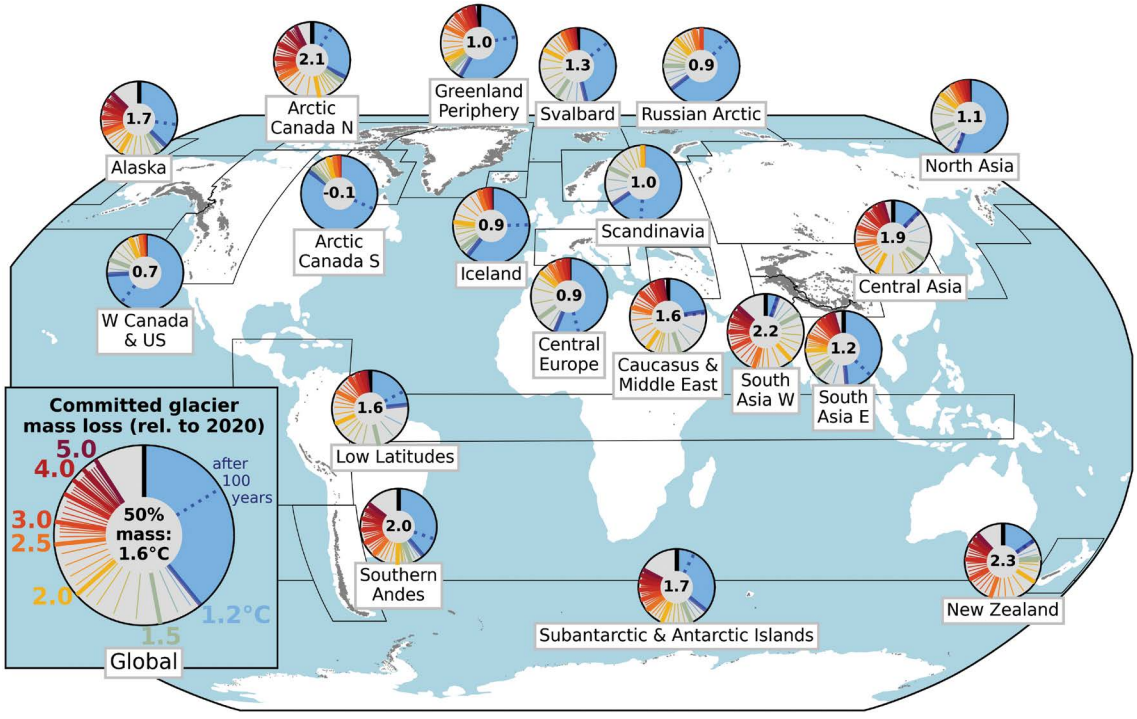

Fig. 3. Committed glacier mass loss at different global warming levels above preindustrial (ΔT). In every circle, the colored lines indicate the LOWESS fitted ensemble median estimates of committed mass loss at steady state at different warming levels in the range ΔT = +1.2°C to +5.0°C (increasing in clockwise directions in 0.1°C steps beyond 1.2°C; full circle correspond to 100% committed mass loss). The present-day committed mass loss at steady state (ΔT = +1.2°C) is in light blue, with the loss after 100 simulation years (fig. S6) shown as the dotted line. Numbers in the circle centers are the ΔT at which 50% of the present (year 2020) regional glacier mass is lost.

Fig. 4. Present-day committed glacier mass loss and response timescales globally and for 19 glacier regions. (**A** and **B**) Present-day committed mass losses (ΔT = +1.2°C) as a function of regional mean glacier elevation range, weighted by glacier area (A), and sensitivity of committed glacier mass loss to global mean air temperature change in the range ΔT = +1.5°C to +3.0°C (B) (see the materials and methods). (**C** and **D**) Response timescale, i.e., the year when 80% of the committed mass loss at ΔT =1.5°C ± 0.2°C has occurred, as a function of glacier-area weighted regional mean surface slope (C) and observed glacier mass change between 2000 and 2019 relative to 2000 (D) (*1*,*37*) (see the materials and methods). *r* is the Spearman's rank correlation coefficient for the 19 regions ($P < 0.02$ in every panel). The coloring of the dots refers to the warming over the glacierized area relative to the global mean warming (versus 1986 to 2005, median value over 80 climate scenarios; Fig. 2). The size of the dots scales with the respective 2020 glacier mass. Slope (C) and observed mass loss (D) data are available in table S3.

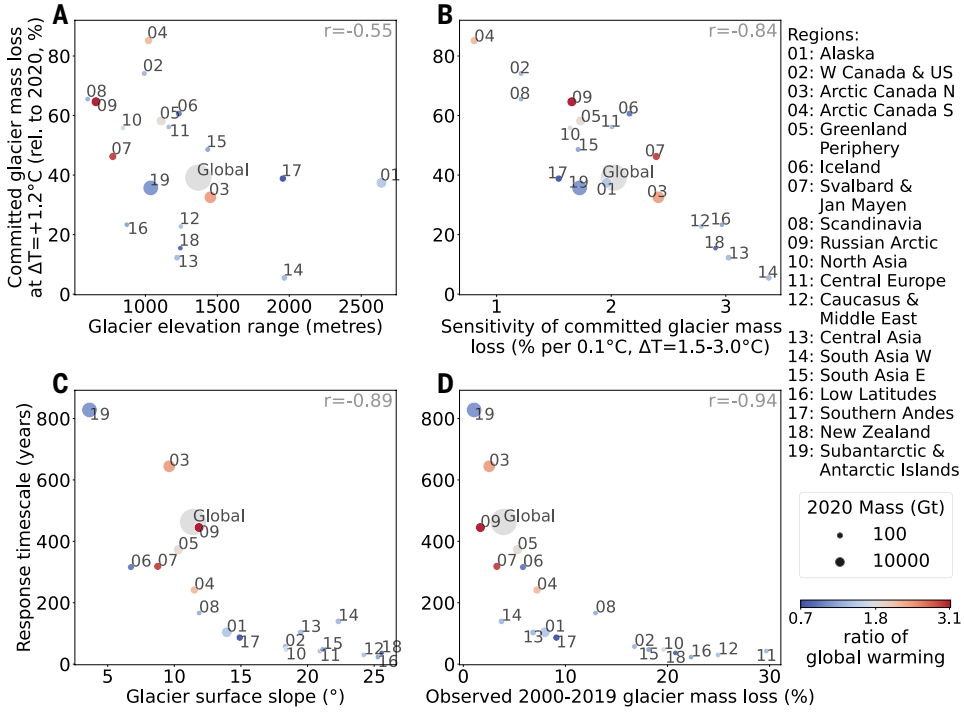

as the Low Latitudes [23 years (range, 14 to 30 years) for 80% change], Caucasus & Middle East [30 years (range, 26 to 56 years)], and New Zealand [36 years (range, 28 to 45 years)]. Under higher warming levels (above +1.5°C), all regions equilibrate faster because they tend to evolve toward a mostly deglaciated state more rapidly (fig. S9B).

The long response timescales result in substantial differences between the glacier states after 100 years and at full equilibration, especially for the slow-responding regions (Fig. 3 and Fig. 2 versus fig. S6). The long-term equilibration experiments thus provide a different and complementary perspective on the vulnerability of glaciated regions compared with previous studies that have focused on transient 21st-century glacier evolution (*10*, *11*). Some regions projected to experience limited mass loss throughout the 21st century, such as the Subantarctic & Antarctic Islands [14% mass loss over 2020 to 2100 for a +2.0°C scenario from an ensemble of three CMIP6-forced glacier evolution models (*11*)], Russian Arctic (22%), and Arctic Canada South (41%), are expected to lose a large part of their mass in the longer term, with committed losses at +2.0°C reaching 56, 88, and 95%, respectively (fig. S10).

Generally, regions modeled to have the longest response timescales are also those with the lowest observed relative mass loss over the past two decades (2000 to 2019), and vice versa ($r = 0.94$; Fig. 4D). For example, the Subantarctic & Antarctic Islands, Arctic Canada North, and Russian Arctic, which each require more than 400 years for 80% of committed changes to occur for a +1.5°C scenario, have lost less than 3% of their mass between 2000 and 2019. By contrast, the fastest responding regions, such as Central Europe, Caucasus & Middle East, Low Latitudes, and New Zealand, need less than five decades for 80% changes to occur and each have lost more than 20% of their mass over the first two decades of the 21st century.

Our results emphasize that the effectiveness of current and near-term climate policies in mitigating short- to mid-term warming will play a decisive role in shaping the future evolution of glaciers, influencing not only immediate glacier changes but also those that will unfold over multicentennial timescales. The findings stress the pivotal role of climate policies in preserving our glaciers, which should be a central focus of the United Nations International Year of Glaciers' Preservation in 2025 (*36*).

REFERENCES AND NOTES

1. R. Hugonnet *et al.*, *Nature* **592**, 726–731 (2021).
2. T. L. Edwards *et al.*, *Nature* **593**, 74–82 (2021).
3. L. Jakob, N. Gourmelen, *Geophys. Res. Lett.* **50**, e2023GL102954 (2023).
4. M. Huss, R. Hock, *Nat. Clim. Chang.* **8**, 135–140 (2018).
5. J. B. Bosson *et al.*, *Nature* **620**, 562–569 (2023).
6. Y. Ding *et al.*, *Earth Sci. Rev.* **213**, 103500 (2021).
7. E. Salim, *Front. Hum. Dyn.* **5**, 1137551 (2023).
8. R. Hock *et al.*, *J. Glaciol.* **65**, 453–467 (2019).
9. B. Marzeion *et al.*, *Earths Futur.* **8**, e2019EF001470 (2020).
10. D. R. Rounce *et al.*, *Science* **379**, 78–83 (2023).
11. H. Zekollari *et al.*, *Cryosphere* **18**, 5045–5066 (2024).
12. J. E. Christian, M. Koutnik, G. Roe, *J. Glaciol.* **64**, 675–688 (2018).
13. B. Marzeion, G. Kaser, F. Maussion, N. Champollion, *Nat. Clim. Chang.* **8**, 305–308 (2018).
14. H. Zekollari, M. Huss, D. Farinotti, *Geophys. Res. Lett.* **47**, e2019GL085578 (2020).
15. J. G. Cogley *et al.*, "Glossary of glacier mass balance and related terms" (IACS Technical Report 86, 2011); https://unesdoc.unesco.org/ark:/48223/pf0000192525.
16. T. Johannesson, C. Raymond, E. Waddington, *J. Glaciol.* **35**, 355–369 (1989).
17. D. B. Bahr, W. T. Pfeffer, C. Sassolas, M. F. Meier, *J. Geophys. Res.* **103**, 9777–9782 (1998).
18. M. Schäfer, M. Möller, T. Zwinger, J. C. Moore, *J. Glaciol.* **61**, 1121–1136 (2015).
19. E. Johnson, S. Rupper, *Front. Earth Sci.* **8**, 8 (2020).
20. G. H. Roe, M. B. Baker, F. Herla, *Nat. Geosci.* **10**, 95–99 (2017).
21. A. Huston, N. Siler, G. H. Roe, E. Pettit, N. J. Steiger, *Cryosphere* **15**, 1645–1662 (2021).
22. O. N. Solomina *et al.*, *Quat. Sci. Rev.* **149**, 61–90 (2016).
23. S. H. Mernild, W. H. Lipscomb, D. B. Bahr, V. Radić, M. Zemp, *Cryosphere* **7**, 1565–1577 (2013).
24. P. M. Forster *et al.*, *Earth Syst. Sci. Data* **16**, 2625–2658 (2024).
25. International Panel on Climate Change, "Climate change 2021: The physical science basis. Contribution of Working Group I to the sixth assessment report of the Intergovernmental Panel on Climate Change" (IPCC, 2021); https://www.ipcc.ch/report/ar6/wg1/.
26. Mountain Research Initiative EDW Working Group, *Nat. Clim. Change* **5**, 424–430 (2015).
27. D. M. Smith *et al.*, *Geosci. Model Dev.* **12**, 1139–1164 (2019).
28. A. Gardner, G. Moholdt, A. Arendt, B. Wouters, *Cryosphere* **6**, 1103–1125 (2012).
29. A. Gilbert *et al.*, *J. Geophys. Res. Earth Surf.* **121**, 1516–1539 (2016).
30. Climate Action Tracker, "The CAT Thermometer" (CAT, 2023); https://climateactiontracker.org/global/cat-thermometer.
31. D. Parkes, B. Marzeion, *Nature* **563**, 551–554 (2018).
32. D. Parkes, H. Goosse, *Cryosphere* **14**, 3135–3153 (2020).
33. F. Paul, T. Bolch, "Glacier changes since the Little Ice Age" in *Geomorphology of Proglacial Systems*, T. Heckmann, D. Morche, Eds. (Springer, 2019), pp. 23–42.
34. G. Roe, J. E. Christian, B. Marzeion, *Cryosphere* **15**, 1889–1905 (2021).
35. B. Marzeion, J. G. Cogley, K. Richter, D. Parkes, *Science* **345**, 919–921 (2014).
36. United Nations, "International year of glaciers' preservation, 2025: revised draft resolution" (UN, 2022); https://digitallibrary.un.org/record/3994297.
37. D. Farinotti *et al.*, *Nat. Geosci.* **12**, 168–173 (2019).
38. Data for: H. Zekollari *et al.*, Glacier preservation doubled by limiting warming to 1.5°C versus 2.7°C, Zenodo (2024); https://doi.org/10.5281/zenodo.14045268.
39. Code for: H. Zekollari *et al.*, Glacier preservation doubled by limiting warming to 1.5°C versus 2.7°C, Zenodo (2024); https://doi.org/10.5281/zenodo.15046031.

ACKNOWLEDGMENTS

We acknowledge the World Climate Research Programme (WCRP) Climate and Cryosphere Project (CliC) for supporting the Glacier Model Intercomparison Project (GlacierMIP). **Funding:** This work was supported by European Union's Horizon 2020 research and innovation program (PROTECT contribution number 158, grant 869304 to H.Z., B.M., M.H., M.J., N.C., T.E., and D.F.); European Research Council under the European Union's Horizon Framework research and innovation program (grant 101115565, ICE^3 to H.Z.); Research Foundation – Flanders (FWO) through an Odysseus Type II project (grant G0DCA23N, GlaciersMD to H.Z. and L.V.T.); VUB ZAP Startkrediet, ICEFIELD (H.Z.); the Austrian Academy of Sciences at the Department of Atmospheric and Cryospheric Sciences, Universität Innsbruck (DOC fellowship 25928 to L.S.); European Union's Horizon 2020 research and innovation program (grant 101003687, PROVIDE to L.S. and F.M.); Norwegian Research Council (project 324131 to R.H.); European Research Council ERC-2022-ADG (grant 01096057 GLACMASS to R.H.); National Aeronautics and Space Administration (grants 80NSSC20K1296 and 80NSSC20K1595 to R.H. and D.R.); Swiss National Science Foundation (grant 200021_184634 to L.C.); Dutch Research Council (NWO) Talent Programme Veni, GREENPEAKS (VI.Veni.222.019 to P.K.); and the NSF National Center for Atmospheric Research, a major facility sponsored by the US National Science Foundation (cooperative agreement 1852977 to W.L., S.M., and G.L.). Computing and data storage resources for CISM simulations were supported by the Derecho system (doi:10.5065/qx9a-pg09) provided by the NSF National Center for Atmospheric Research (NCAR), sponsored by the National Science Foundation (W.L., S.M., and G.L.); GRICAD infrastructure (N.C.); European Research Council under the European Union's Horizon Framework research and innovation program (grant 101142123, DROP, to W.I.); and the World Climate Research Programme (WCRP) Climate and Cryosphere Project (CliC), which funded GlacierMIP workshops. **Author contributions:** H.Z. and L.S. contributed equally to this work and share first authorship. H.Z. was the main project coordinator of the study, which initiated from original ideas by B.M. H.Z., L.S., F.M., R.H., and B.M. designed the GlacierMIP3 experiments, protocol, and methods. F.M., R.H., B.M., and H.Z. acquired funding for data analyses and GlacierMIP3 activities. F.M. did exploratory simulations and analyses to guide the GlacierMIP3 experimental design choices. L.S. preprocessed the climatic input data for the model experiment in close collaboration with F.M. F.M., L.S., and H.Z. created test files and example workflows and guided the data submission process. L.C., K.F., M.H., M.J., P.K., W.L., F.M., S.M., M.O., D.R., L.S., L.V.T., and H.Z. performed the GlacierMIP3 model experiments with contributions in form of supervision and feedback by T.E., D.F., W.I., G.L., and A.S. L.S. performed all data analyses, including pre- and postprocessing of the submitted model simulations and made the figures in close collaboration with H.Z. and F.M. with additional input from R.H., B.M., and D.R. L.S. curated and validated data with input from F.M. B.M. provided resources for computation and data storage. H.Z. and L.S. interpreted the results with input from F.M., R.H., and B.M. H.Z. wrote the original manuscript with major contributions from R.H. and L.S. F.M., D.R., and B.M. provided extensive text reviews and edits, with additional contributions from N.C., L.C., K.F., W.I., P.K., W.L., S.M., L.V.T., and particularly M.H. and D.F. **Competing interests:** The authors declare no competing interests. **Data and materials availability:** The submitted data from the glacier model groups and the code to reproduce the figures is available from (*38*,*39*).

SUPPLEMENTARY MATERIALS

science.org/doi/10.1126/science.adu4675
Materials and Methods; Figs. S1 to S15; Tables S1 to S3; References (*40*–*66*)

Submitted 8 November 2024; accepted 2 April 2025

10.1126/science.adu4675

Science
AAAS

Supplementary Materials for

Glacier preservation doubled by limiting warming to 1.5°C versus 2.7°C

Harry Zekollari *et al*.

Corresponding authors: Harry Zekollari, harry.zekollari@vub.be; Lilian Schuster, lilian.schuster@uibk.ac.at

Science **388**, 979 (2025)
DOI: 10.1126/science.adu4675

The PDF file includes:

Methods

Experimental setup

We analyzed simulations from eight large-scale glacier evolution models (Table S 2) performed as part of the third phase of the Glacier Model Intercomparison Project (GlacierMIP3 (*38*)), an activity of the World Climate Research Program's Climate and Cryosphere Project (WCRP CliC). All models calculated the annual regional glacier mass evolution in response to a range of constant-climate scenarios (detailed in 'Climate scenarios' section) by simulating either all individual glaciers in a region or a subset (with results then upscaled to represent the entire region).

Each model was calibrated using mass-balance observations and meteorological reanalysis data chosen by the modeler. Glacier models differed in their initialization strategies (Table S 2) but all aimed to match glacier areas from the Randolph Glacier Inventory (RGI6.0 (*40*)) and glacier volumes from Farinotti et al. (*37*), either for each RGI region or, where possible, for individual glaciers. The initial areas and volumes are based on data from approximately the year 2000.

For consistency, regional volume time series were scaled (multiplication with constant value) to exactly match the estimates by Farinotti et al. (*37*) at the start of the simulation. Most models were then run for 2000 or 5000 years depending on the region to ensure sufficient time for the glaciers to equilibrate under the given climate scenarios (see section 'Glacier mass time series and steady state'). Glacier volume was converted to mass assuming an ice density of 900 kg m^{-3}.

Climate scenarios

The climate scenarios were derived from transient climate simulations from five global climate models from the Coupled Model Intercomparison Project Phase 6 (CMIP6) as provided by the Inter-Sectoral Impact Model Intercomparison Project (ISIMIP 3b): GFDL-ESM4, IPSL-CM6A-LR, MPI-ESM1-2-HR, MRI-ESM2-0, and UKESM1-0-LL. All glacier models required monthly near-surface air temperature and precipitation as forcing data, while one model also required daily resolution and additional variables (relative humidity, wind speed, and downward solar radiation, Table S 2).

Constant-climate scenarios were generated by repeating 80 different 20-year periods of climate data for the entire simulation of 2000 or 5000 years. Specifically, each of the five climate models provided 16 different 20-year subsets of climate data that included four periods from the past (1851-1870, 1901-1920, 1951-1970, 1995-2014) as well as four in the future (2021-2040, 2041-2060, 2061-2080, 2081-2100) for three different Shared Socioeconomic Pathways (SSPs; SSP1-2.6, SSP2-4.5, and SSP5-8.5) (Fig. S 1). To avoid cyclicity in the glacier mass time series, the years within each 20-year repeat period were shuffled according to a prescribed randomized order, with a different shuffling at every repeat cycle. Thus, the climate in each scenario was kept constant while allowing for varying interannual variability.

Definition of warming levels

Each climate scenario corresponds to a constant climate at a given global warming level (Fig. S 1). Following the Sixth Assessment Report of the International Panel on Climate Change (IPCC) (*25*), for each of the 80 climate scenarios, the global warming level above pre-industrial was computed from the difference between the global average of each 20-year repeat period and the average over the period 1986-2005, to which 0.69°C was added to account for the warming between pre-industrial (1850-1900) and the 1986-2005 period. We note that Rounce et al. (*10*), used a slightly different value (+0.63°C) based on a previous IPCC report (*41*). The mean global warming levels above pre-industrial of the climate scenarios ranged from -0.1°C (Fig. S 1B, IPSL-CM6A-LR) to +6.9°C (Fig. S 1B, UKESM1-0-LL).

Note that two climate scenarios with the same mean global warming level may project different global and regional glacier mass losses due to different spatial and temporal patterns. The spatial and temporal variability in our synthetic climate scenarios, extracted from transient climate model simulations, can also be expected to be different from the true climate system response at comparable global warming levels due to non-linear feedbacks in the climate system (*42*, *43*).

Present-day committed losses were estimated using the +1.2°C scenario, since the global warming level above pre-industrial reached 1.2°C in the period 2014-2023 (*24*). To determine warming levels over the glacierized terrain (ΔT_g; Fig. S 4), we selected the climate model grid points nearest to each glacier´s RGI center coordinates and calculated the regionally and globally averaged warming weighted by the glacier area at the inventory date, assuming the same warming of +0.69°C between pre-industrial (1850-1900) and 1986-2005 as the global average. To calculate the ratio of regional warming over glacierized areas relative to the global mean, we computed the warming relative to 1986-2005 rather than 1850-1900, since data of the warming between these periods were not available for the individual RGI glacier regions (ΔT^*, Fig. 2, Fig. 4, Fig. S 2).

Glacier mass time series and steady state

Glacier simulations were performed over the full 2000- or 5000-year period with a few models stopping their per-glacier simulations upon detecting a steady state for glacier mass earlier (i.e., before end of full 2000- or 5000-year period; Table S 2; Table S 3). Similar to Ziemen et al. (*44*), we assumed the glacier mass of each region has reached a steady state when the absolute mass change over a 20-year repeat period is less than 0.5% of the total absolute mass change relative to 2020 (Fig. S 8). This criterion was applied using 101-year rolling averages, and allowed detecting steady states without being oversensitive to the multi-centennial variability from the constant, but random climate. With this definition, steady state was reached by the end of the simulation period for the vast majority (97%) of the 7360 model experiments (4-6 glacier models for 19 regions with 80 climate scenarios each). Therefore, we calculated steady-state regional glacier mass as the mean of the last 101 years of the full simulation period.

Committed mass losses for different global warming levels

For each warming level and region, we determined the mass losses between steady-state and present-day glacier mass (defined here as year 2020). While the term “committed” often refers to the losses in response to current climatic conditions (assumed to remain constant) (*23*, *12*,

14), here we expand its meaning to include the mass losses in response to a range of global warming levels.

To determine the glacier volume in 2020 (later converted to mass) we accounted for the volume changes that have occurred between the start of the simulations (based on regionally varying RGI dates centered around 2000) and the beginning of 2020 (Table S 3). To do so, we used regional geodetic volume change observations (*1*) averaged over four 5-year periods (2000-2004, 2005-2009, 2010-2014, 2015-2019), and assumed these values to be constant over the 5-year period. Since the years that individual glaciers refer to in the RGI vary, for each region we used the median area-weighted RGI-year of all glaciers, $\mathrm{yr_{RGI}}$ (Table S 3), and computed regional glacier volume in 2020 (V_{2020}) by:

$$V_{2020} = V_{yr_{RGI}} + \sum_{i=yr_{RGI}}^{2019} \Delta V_i, \qquad \text{(Eq. 1)}$$

where ΔV_i is the observed annual volume change for each year *i* ranging from each region´s yr_{RGI} to the year 2019. For regions where yr_{RGI} is before 2000 (Subantarctic & Antarctic Islands (1986), New Zealand (1978), and Arctic Canada North (1999)), we assumed no volume changes before 2000 consistent with relatively balanced conditions for these three regions before 2000 (*45*). We used the same approach to estimate regional glacier volumes in the year 2000 (Table S 3), which are needed to derive the 2000-2019 regional changes (e.g., Fig. 4D).

Response timescale

As a measure to evaluate the time required for regional and global glacier mass to equilibrate relative to the mass in 2020, for each experiment we calculated the number of years needed to reach 80% of the committed mass change (henceforth referred to as response timescale; Fig. S 11). This timescale differs from the definition of response time which describes the e-folding timescale for transitioning a glacier from one steady state to another in response to a step change in mass balance (*15*). To accommodate the asymptotic nature of mass evolution, we opted for an 80% threshold of committed mass change, which is close to glacier stabilization and thereby ensures that the mass changes over consecutive 21-year periods surpass the noise stemming from interannual variability.

We applied the criterion on a 21-year centered rolling average to remove random variability while ensuring not to artificially inflate the response timescales, which could be the case with longer rolling periods. We only considered those experiments where at least 25% of the glacier mass in 2020 was lost by the end of the simulation period. This threshold was necessary to account for warming level changes close to the pre-industrial level where the interdecadal variability hampers a response timescale analysis.

To estimate regional response timescales for each experiment (combination of glacier model and climate scenario), we shifted each time series in time (by a maximum of 50 years) so that the regional mass is closest to the regional mass in 2020 (instead of the mass at the RGI date). The resulting year is redefined as the new starting point of the time series (simulation year 0 in Fig. S 12) and used to calculate the response timescale. The shift was necessary since our simulations started prior to 2020. This shift is particularly important to consider in regions with short response timescales where the glacier mass has significantly decreased between the start of the simulations and 2020.

Estimating steady-state mass across warming levels

A locally weighted scatterplot smoothing (LOWESS (*46*)) fit was employed to establish the relationship between the steady-state glacier mass and any given warming level using the 'moepy' python package (*47*). Regionally, the LOWESS fit was performed over results from all applied glacier models. For instance, in regions where five glacier models were applied, this involved fitting 400 data points (five glacier models each with 80 constant-climate scenarios). Globally, the LOWESS fit was performed over the sum of the medians of each RGI region, thereby also incorporating data from glacier models that were only applied in certain regions. In all cases, the number of robustifying iterations ("robust_iters") was set to 2.

For the median fit (LOWESS quantile regression at 50th percentile) of each region and globally, we considered fits with "frac" (fraction of data) parameters in a range of 0.1 to 1 (in 0.01 steps). We selected the fit with the lowest root-mean squared error that was monotonically decreasing with global warming levels and non-negative. When a monotonically decreasing non-negative fit could not be obtained, we selected the least negative fit that was still monotonically decreasing. If none of the fits were monotonically decreasing, we selected the least locally increasing fit. Any negative mass values were set (i.e., "clipped") to zero. For comparison, we also show an exponential fit, adopting a robust least-square optimization from 'scipy' (*48*) to reduce the weight of outliers (e.g., Fig. 1B, Fig. 2). The results presented in figures and tables are derived from the LOWESS fits, as the exponential fit not deemed suitable for higher warming levels in some regions, specifically after 100 simulation years (Fig. S 6).

Uncertainty quantification

Uncertainty estimates were computed to represent the IPCC (*25*) 'likely' range (17th and 83rd percentiles) by calculating LOWESS fitted quantile regressions. This approach was favored over using the standard deviation because the glacier model sample size was small (4 to 6 models per RGI region), and the results did not necessarily follow a Gaussian distribution.

The percentiles were calculated using the same "frac" parameter as for the median fit (see above). Here also, the fits were clipped to zero. If the percentiles were locally decreasing followed by an increase, rather than maintaining a monotonic decrease, we replaced those values with the local maximum corresponding to the next higher warming level (in 0.05°C increments). This correction was applied since these minor local minima result from sampling variability and lack a physical interpretation.

Since not all eight glacier models were applied globally (Fig. 2, Table S 2), for the global uncertainty, we created composite regions with projections of the same glacier model ensemble. Specifically, we first summed the glacier model estimates for the regions that were only modelled by the four global glacier models (regions 01, 03, 04, 05, 07, 09, 17, 19). We then repeated this process for regions that where modelled by the global models and GloGEMflow3D (regions 02, 08, 10, 12, 16, 18), the three regions in High Mountain Asia that were also modelled by the Kraaijenbrink model (regions 13, 14, 15), Iceland (region 06, modelled by global models, GloGEMflow3D and GO), and Central Europe (region 11, modelled by global models, GloGEMflow3D and CISM2). For each of these five composite regions, we computed a LOWESS fit and summed the 17th and 83rd percentiles. Assuming a perfect correlation between the composite regions this approach results in conservative global

uncertainty estimates, providing an upper bound on overall uncertainty. Nevertheless, by using the adopted composite regions, we account for some balancing effects, where certain glacier models project the most glacier mass loss in some regions while projecting the least loss in others.

Impact of regionally varying glacier model ensemble composition

To evaluate the effect of varying glacier model ensemble composition across regions on regional and global results, we also computed the LOWESS fits and uncertainties by exclusively utilizing the simulations from the four global models. We note that 90% of the glacier mass in 2020 is located in regions that are modelled only by the four global models. Generally, we found that the choice of model ensemble composition had little influence on median regional and global steady state and response timescale characteristics. For example, we estimate a global committed mass loss of 38 [14 to 55] % for the +1.2°C scenario using only the four global models (Fig. S 13; relying on global values), which is within 1% of the median loss and uncertainty range based on summing the composite region's percentiles (reference estimate, Table S 1).

Sea-level contribution

Global glacier mass loss was converted into sea-level contribution (*15*) using an ocean area of 3.625×10^8 km², an ice density of 900 kg m^{-3} and an ocean density of 1028 kg m^{-3}. Since most of the glacier ice lost below sea level does not contribute to sea level rise because it already displaces ocean volume, we subtracted these losses from our regional mass loss estimates prior to converting the mass change to sea level equivalent. To do so, we used results from the Open Global Glacier Model (OGGM (*49*)), the only global glacier model that estimated each glacier´s steady-state glacier mass above and below sea level separately.

For all 80 climate scenarios, we computed the fraction, *F*, of steady-state mass above sea level relative to the steady-state total glacier mass. A linear regression between *F* and the total steady-state mass was derived to account for temporal variations (Fig. S 14). Specifically, *F* increases with decreasing steady-state glacier mass consistent with marine-terminating glaciers eventually retreating onto land (Fig. S 14). *F* varies between 0.89 and 0.94 for the climate scenarios corresponding to the +1.2°C to +4.0°C range. For all experiments we used the linear fit to determine *F* for the mass in 2020, F_{2020}, and for the steady-state mass, $F_{steady-state}$, and computed the median mass above sea level M_{ASL} by:

$$M_{ASL} = M_{2020} \times F_{2020} - M_{steady-state} \times F_{steady-state}, \quad \text{(Eq. 2)}$$

For the 17th and 83rd percentiles, we used the corresponding percentiles of total glacier mass loss and added a sea-level rise conversion uncertainty by applying a fraction *F* of 0.8 for the lower bound and 1.0 for the upper bound.

Sensitivity of committed glacier mass loss to global warming

We evaluated global and regional mass change sensitivities, here defined as the relative change in committed glacier mass loss with respect to glacier mass in 2020 (in %) per 0.1°C global mean temperature change. In practice, we calculated the sensitivity from the difference between the LOWESS fitted relative glacier mass remaining at the +1.5°C and +3.0°C warming levels (Fig. 1B, Fig. 2). These warming levels were chosen since the remaining mass (in %) is almost linearly correlated with global warming levels in this range. In addition, the +1.5 to 3.0°C range

includes the +1.5°C and +2.0°C levels of the Paris agreement goals and the +2.7°C level anticipated under current policies (*30*). To estimate uncertainties, we calculated sensitivities from the climate scenarios for each glacier model individually (Fig. S 5). We calculated the 17th and 83rd percentiles from the ensemble that included both the sensitivities of each glacier model and the results from fitting all glacier models together.

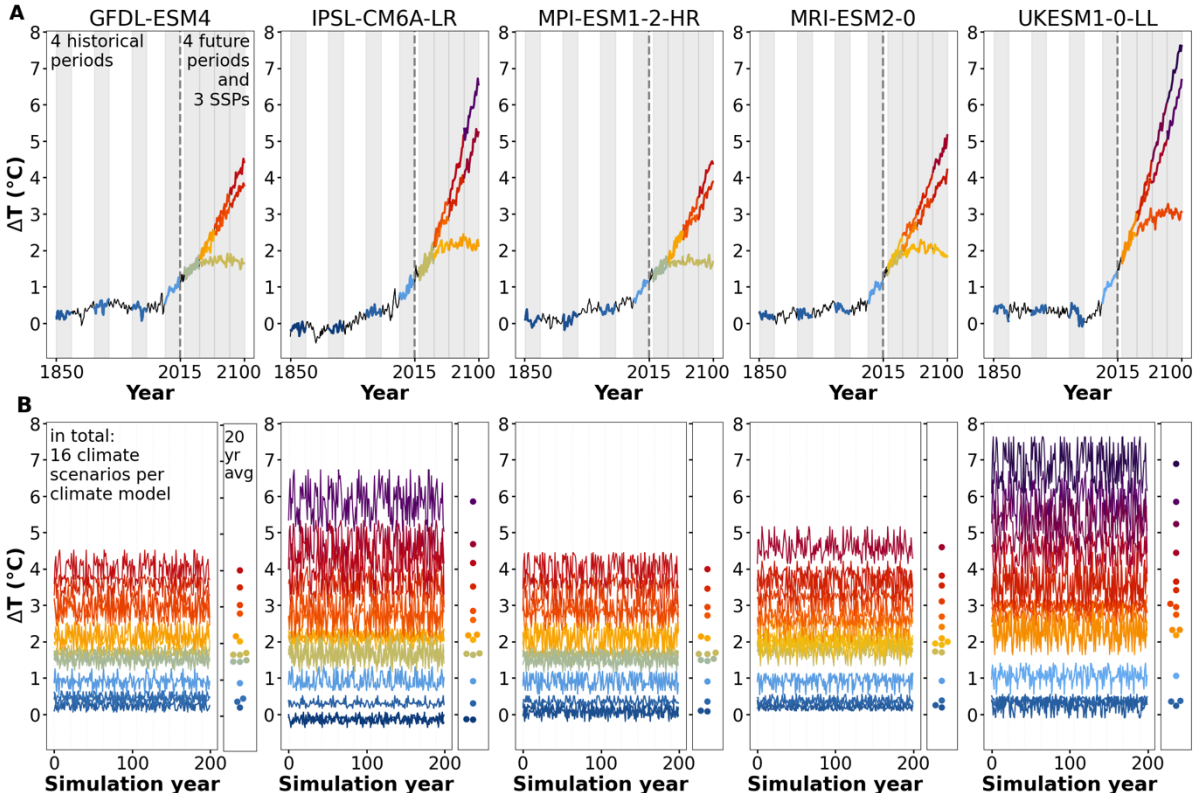

Fig. S 1. Overview of air temperature forcing for the 80 constant-climate scenarios. (**A**) Global mean annual near-surface air temperatures above pre-industrial (ΔT) between 1850 and 2100 for the five ISIMIP3b climate models, and after 2015 for three SSPs (SSP1-2.6, SSP2-4.5 and SSP5-8.5). 20-year historical (1851-1870, 1901-1920, 1951-1970, 1995-2014) and future (2021-2040, 2041-2060, 2061-2080, 2081-2100) periods were used to extract the climate forcing for the glacier models. (**B**) Derived climate scenarios used to force the glacier models, shown for the first 200 simulation years (left subpanels with lines), together with mean ΔT (right subpanels with dots).

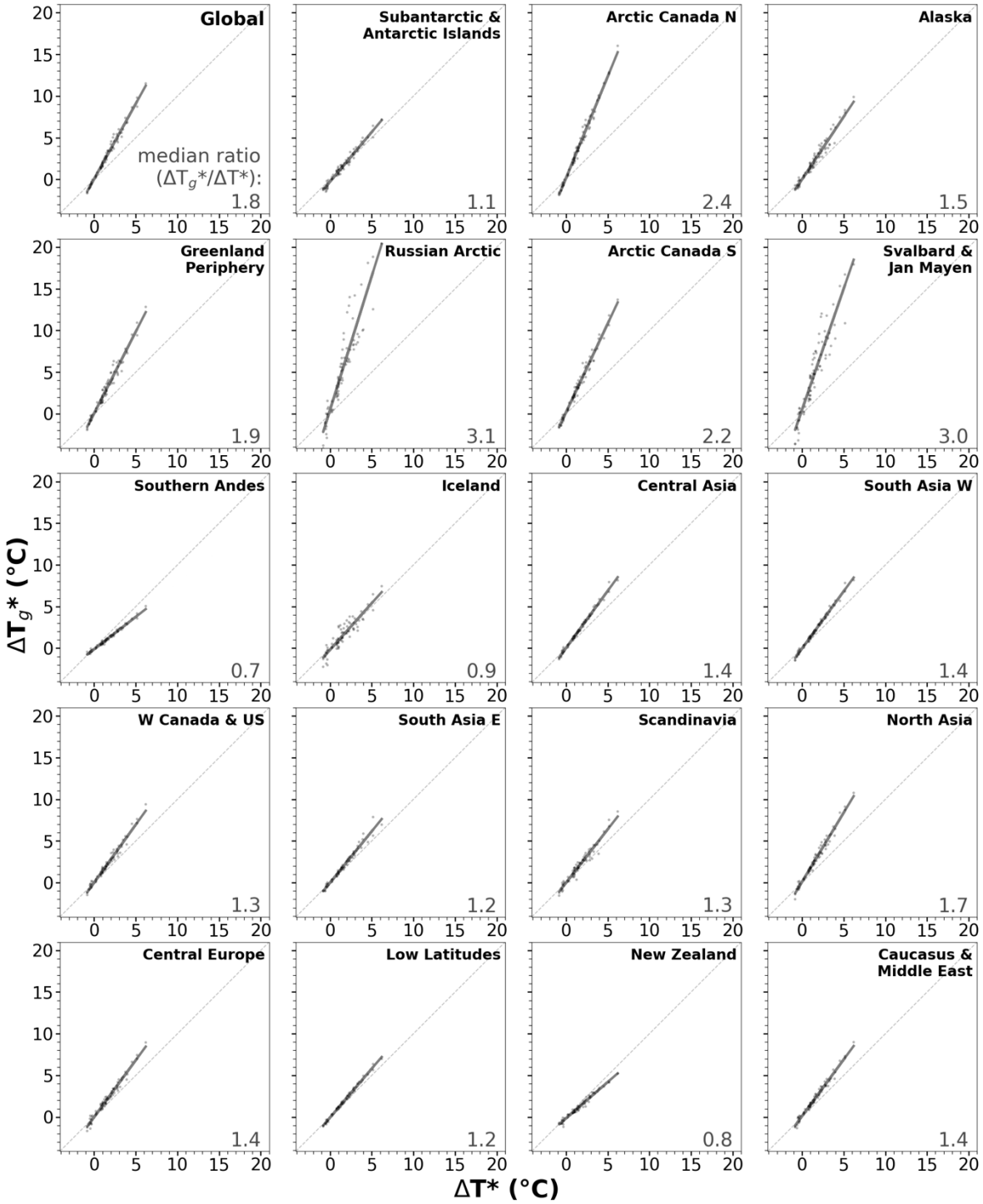

Fig. S 2. Global and regional glacier-area weighted warming (ΔT_g*) as a function of global warming (ΔT*), relative to 1986-2005. Each panel represents a specific region (ordered by present-day volume), showing values for the entire global warming level range, where every dot corresponds to a climate scenario. See Methods for details.

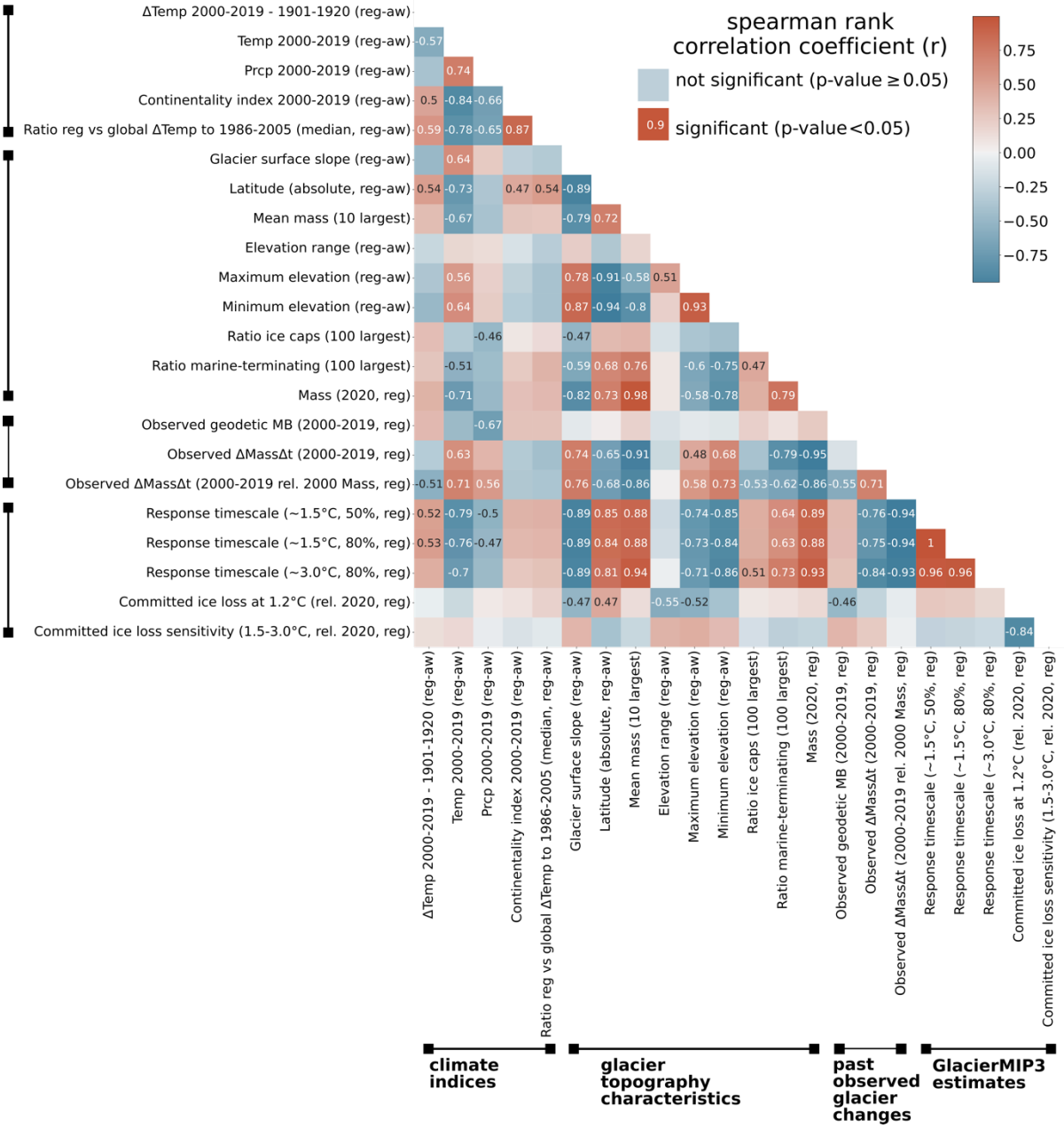

Fig. S 3. Correlation coefficients between regional climate indices, glacier topography characteristics, past glacier changes and steady-state and temporal response behavior. Characteristics are shown for every category, with significant ($p<0.05$) Spearman rank correlation coefficients (r) annotated. Correlations were estimated from aggregated regional estimates (19 values). Climate data is from ISIMIP3a (GSWP3-W5E5 (*50*)). The continentality index is the temperature difference between the coldest and warmest month of the same year, averaged over 2000-2019. Past observed glacier changes are from Hugonnet et al. (*1*) Abbreviations: "10/100 largest" refers to the 10/100 glaciers with the largest initial glacier mass at inventory date according to Farinotti et al. (*37*), "reg-aw" refers to regionally glacier-area weighted, "reg" to regional, "avg" to average, "Temp" to temperature and "Prcp" to precipitation.

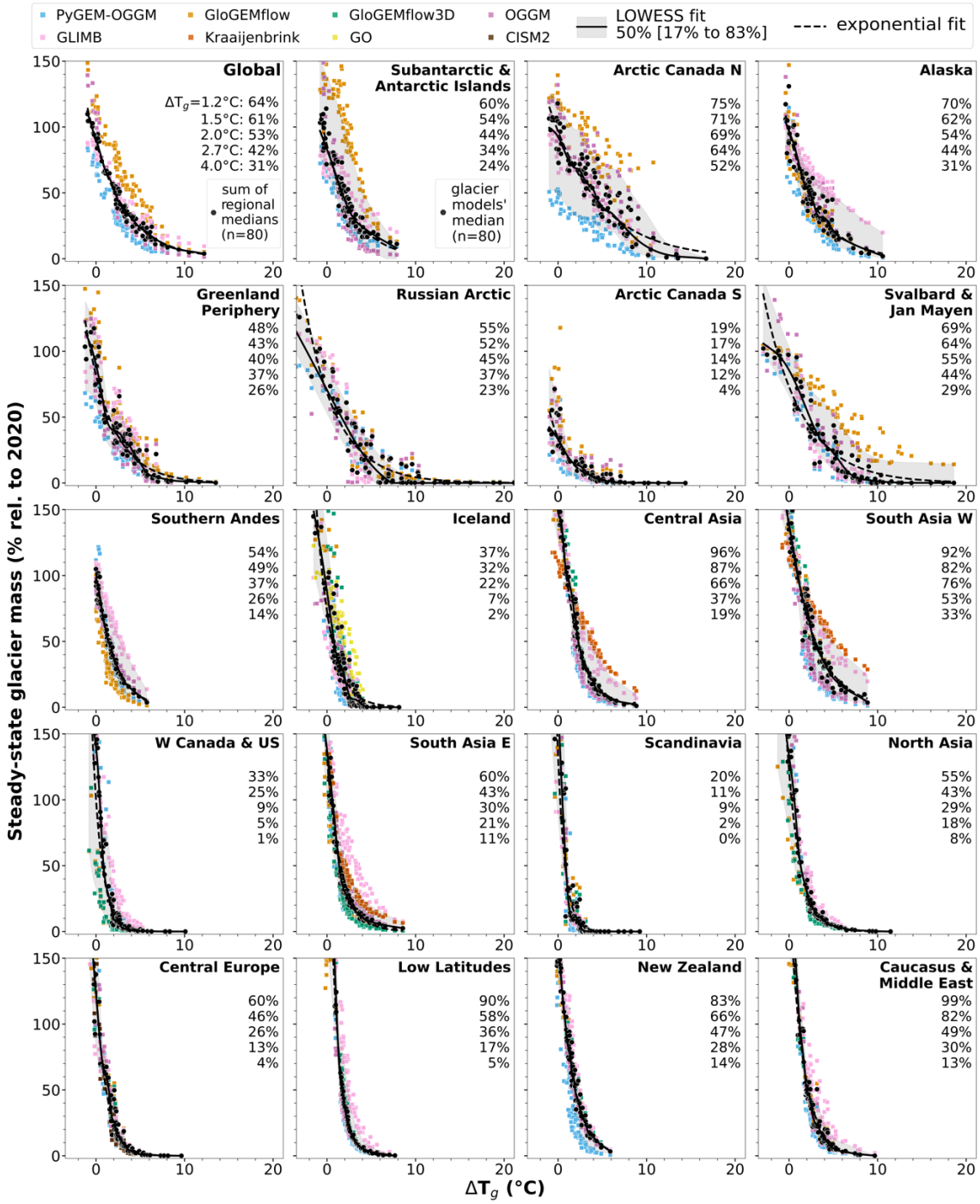

Fig. S 4. Steady-state glacier masses relative to present-day (year 2020) as a function of warming levels over each region's glacierized area (ΔT_g). Dots represent individual simulations forced by 80 climate scenarios per glacier model (4-6 glacier models per regions, color-coded). Regions are sorted by descending present-day (2020) glacier mass. Numbers in the subplots are the steady state relative glacier masses relative to present-day for distinct warming levels (refer to 'Global' panel for the warming levels). The x-axis is clipped at the minimum and maximum ΔT_g values. Regional warming levels were determined using the same $\Delta T = +0.69°C$ between pre-industrial (1850-1900) and 1986-2005 as for global warming levels (see Methods). Uncertainty ranges (17^{th} to 83^{rd} percentile) from the LOWESS fit are shaded in grey. There are no uncertainty estimates for the global estimate since regional uncertainties cannot be summed up due to dependence on regional, not global, glacier-area weighted warming levels.

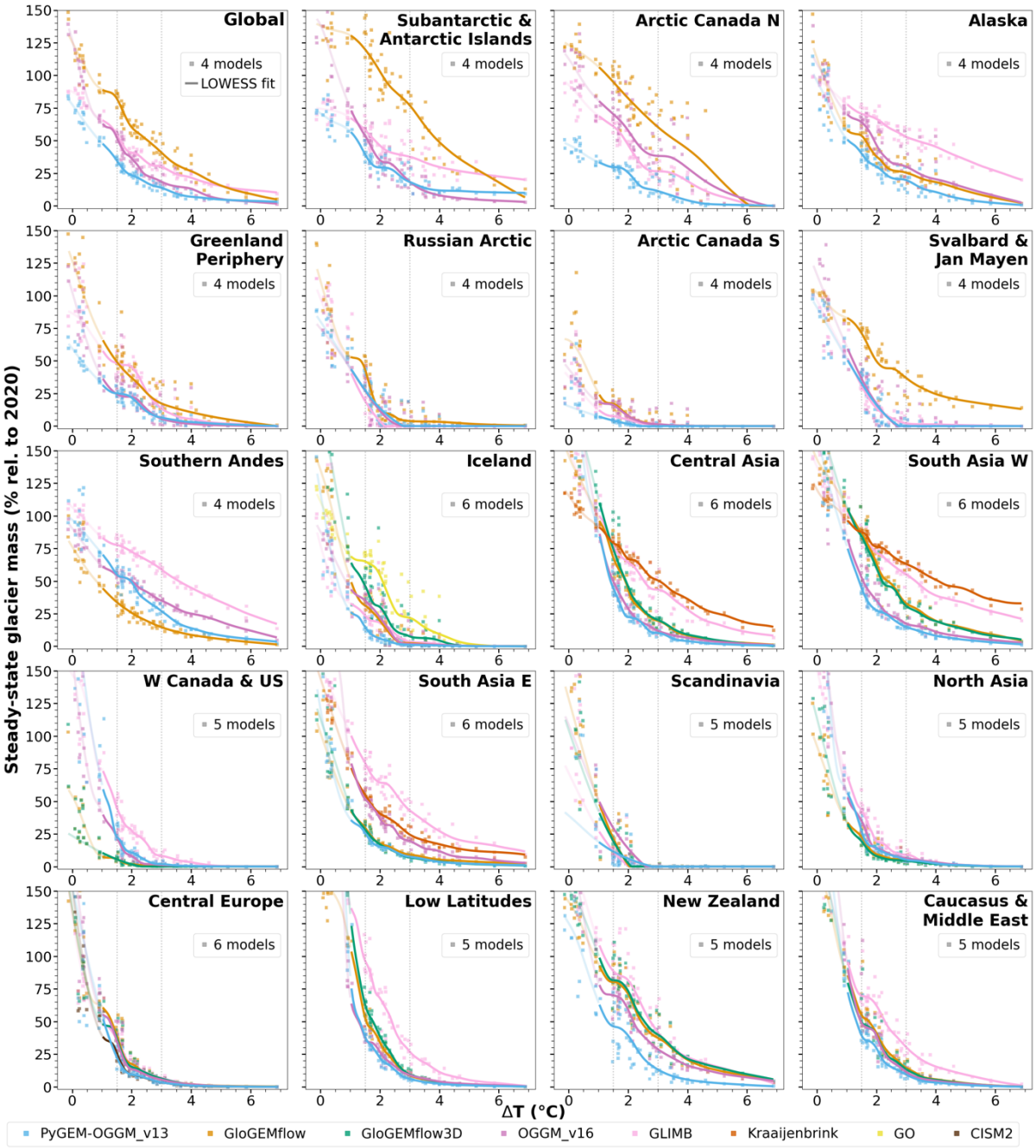

Fig. S 5. Steady-state per-glacier-model glacier masses relative to present-day (year 2020) as a function of global warming levels above pre-industrial (ΔT). This figure shows LOWESS fits of individual glacier model results, as opposed to the (summed) multi-model median in Fig. 1B, Fig. 2. This fit here is used to estimate the uncertainty of the sensitivity to global warming levels at 1.5°C and 3.0°C (Table S 1). The fits below the 1.0°C warming level are shown as transparent to illustrate that in some cases the fit does not represent the model behavior closely. Dots represent individual simulations forced by 80 climate scenarios per glacier model (4-6 glacier models per region, color-coded). Regions are sorted by descending present-day (2020) glacier mass.

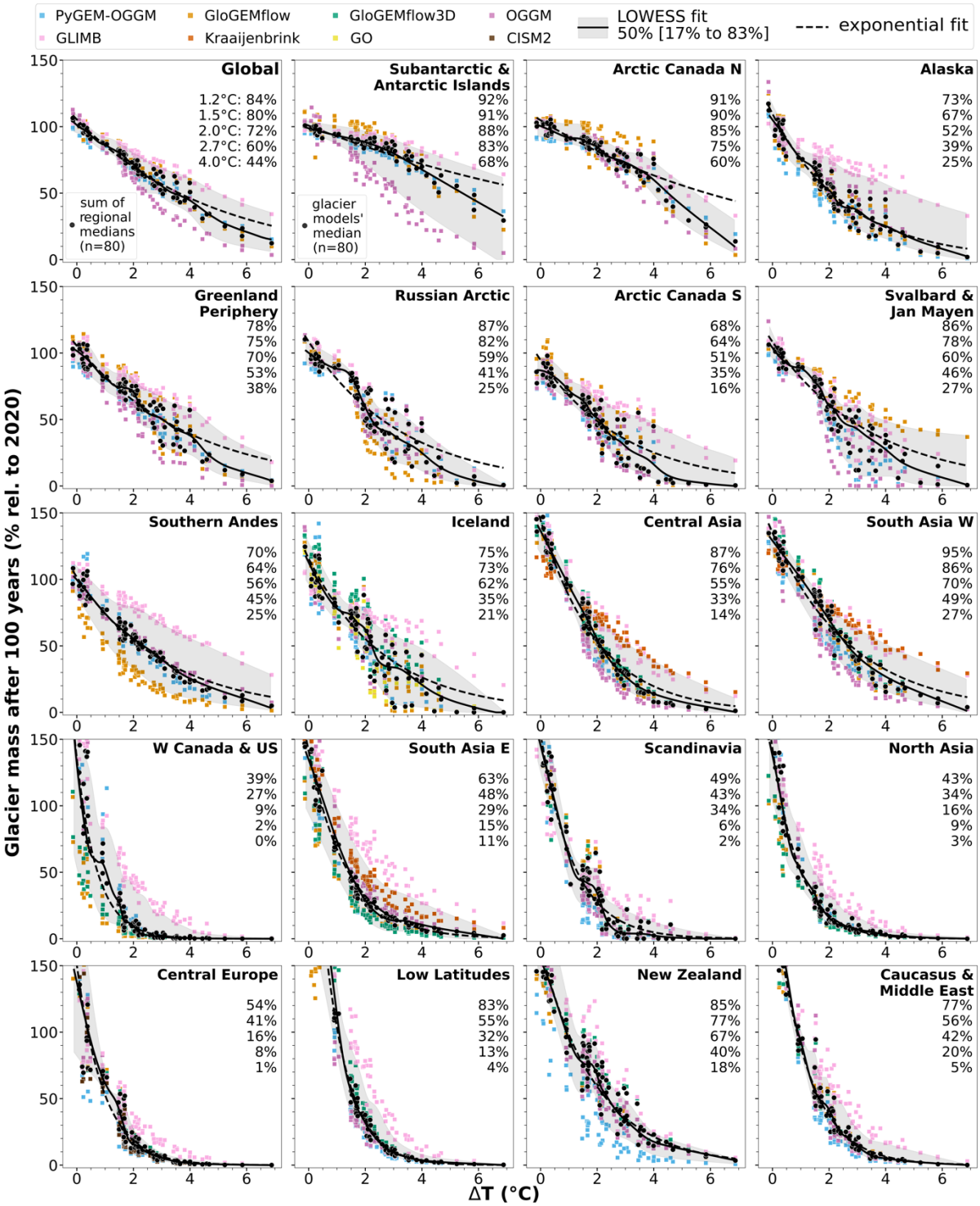

Fig. S 6. Glacier masses after 100 simulations years relative to present-day (year 2020) as a function of global warming levels above pre-industrial (ΔT). Dots represent individual simulations forced by 80 climate scenarios per glacier model (4-6 glacier models per region, color-coded). Regions are sorted by descending present-day (2020) glacier mass. The rolling mass average is taken over 21 years. Numbers in the subplots are the glacier masses in percent after 100 simulation years relative to present-day for distinct warming levels (see 'Global' panel for the warming levels).

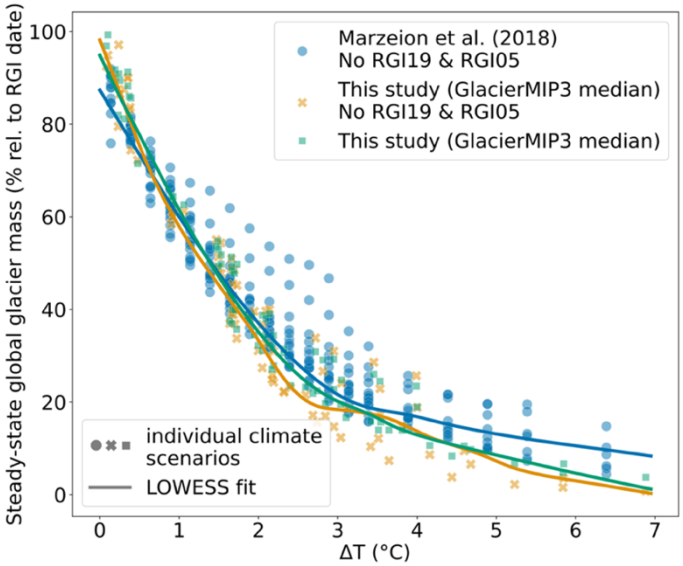

Fig. S 7. Sensitivity of committed global glacier mass loss to global mean warming levels above pre-industrial, compared to Marzeion et al. (*13*). For direct comparison, estimates are shown relative to the simulation start (RGI date) instead of 2020 as in the main text. In Marzeion et al. (*13*), about 60% of the global glacier mass is simulated, excluding Subantarctic & Antarctic Islands (RGI19) and the Greenland Periphery (RGI05).

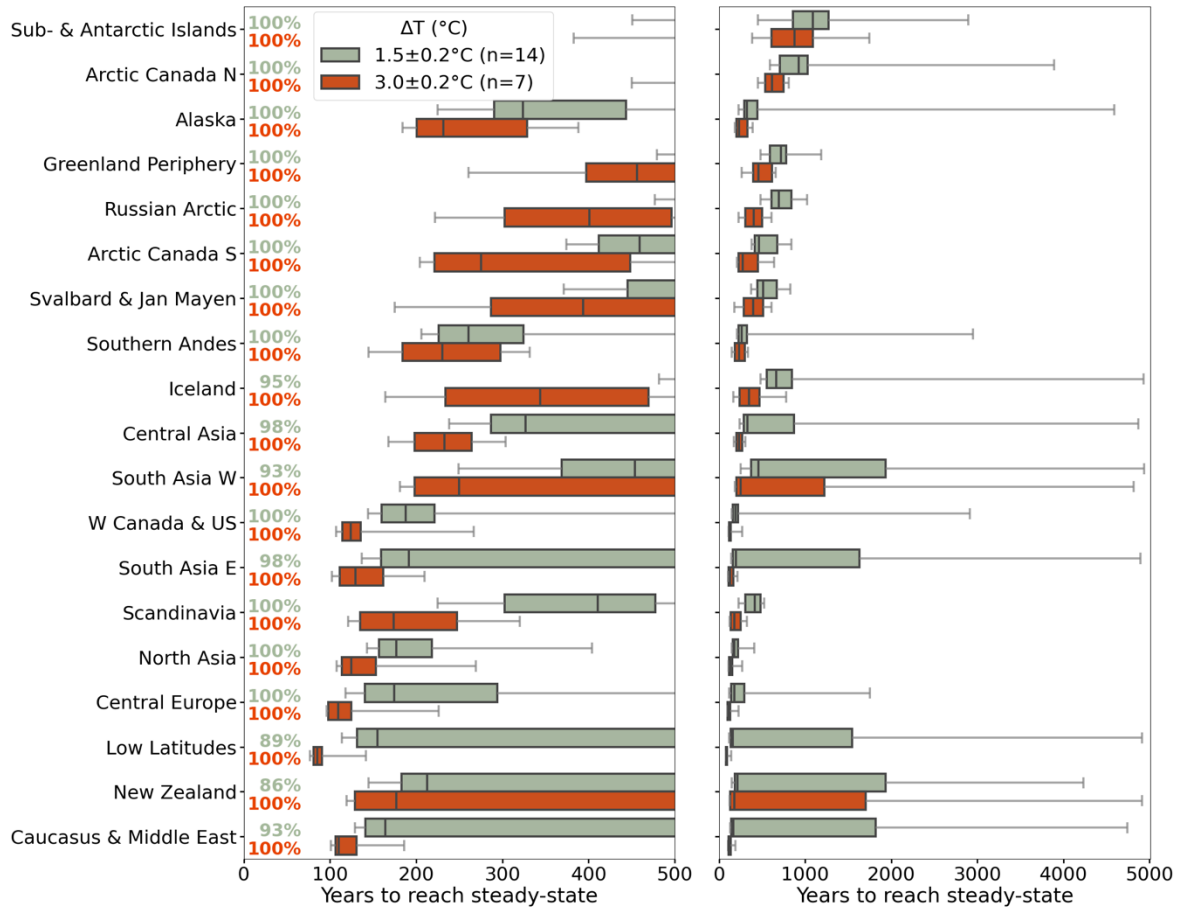

Fig. S 8. Years to reach steady state. For each region, percentiles (5th, 25th, median, 75th, 95th) are calculated over the individual "year estimates" of the glacier models and climate scenarios (see Methods). In the left panel, the percentage of experiments (glacier model and climate scenario combinations) reaching steady state is highlighted (considering all climate scenarios, i.e. also those with little changes). Due to the 101-year rolling average, the steady state can be reached earlier than estimated under very fast-responding climate scenarios, regions and glacier models. *n* in legend refers to the number of climate scenarios.

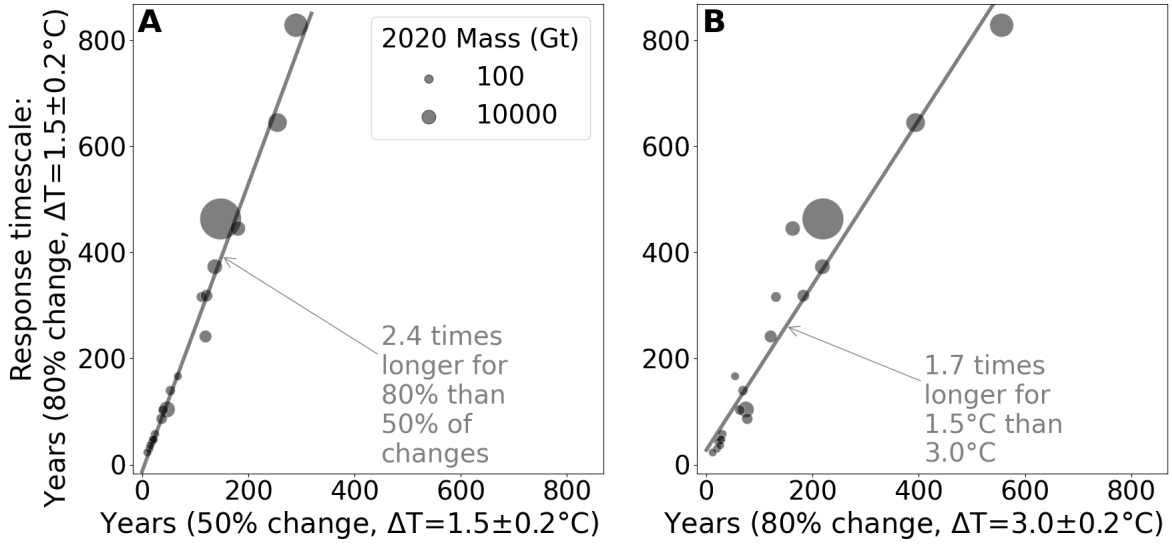

Fig. S 9. Response timescale in years after simulation start for different timescale definitions. Time when 80% of the committed mass loss has occurred at ΔT=1.5°C compared to (**A**) the estimates for 50% losses (Fig. S 11 vs. Fig. S 15) and (**B**) the estimates at ΔT=3.0°C. Each dot represents one of the 19 RGI regions. The size of the dots scals with the respective 2020 glacier mass.

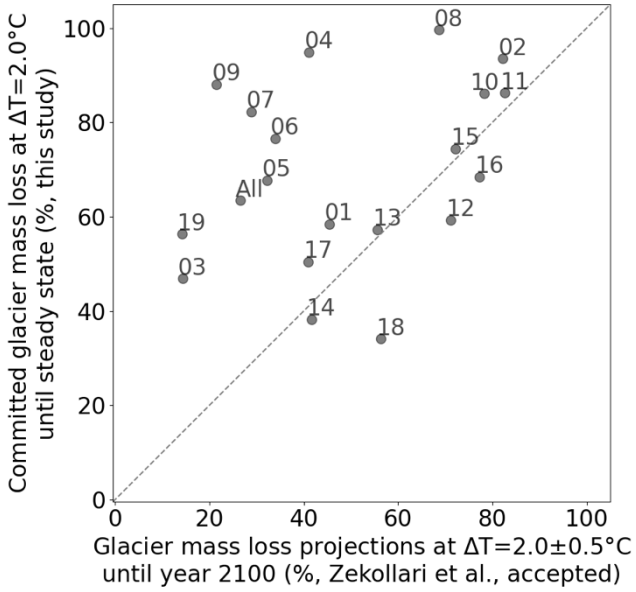

Fig. S 10. Committed glacier mass loss (in %, relative to 2020) from equilibration experiments (this study) versus mass losses by 2100 relative to 2015 derived from transient climate projections (*11*)**.** For the equilibration experiments in this study, results are shown for ΔT = 2.0°C (median LOWESS fit). The 21st century glacier projections are from Zekollari et al. (*11*), representing the median of three global glacier models (PyGEM-OGGM, OGGM, GloGEM) and of 17 climate model and SSP combinations of CMIP6 within the ΔT = 2.0°C±0.5°C range. "All" indicates the global losses, while the numbers refer to the RGI region numbers (refer to Table S 3 for naming).

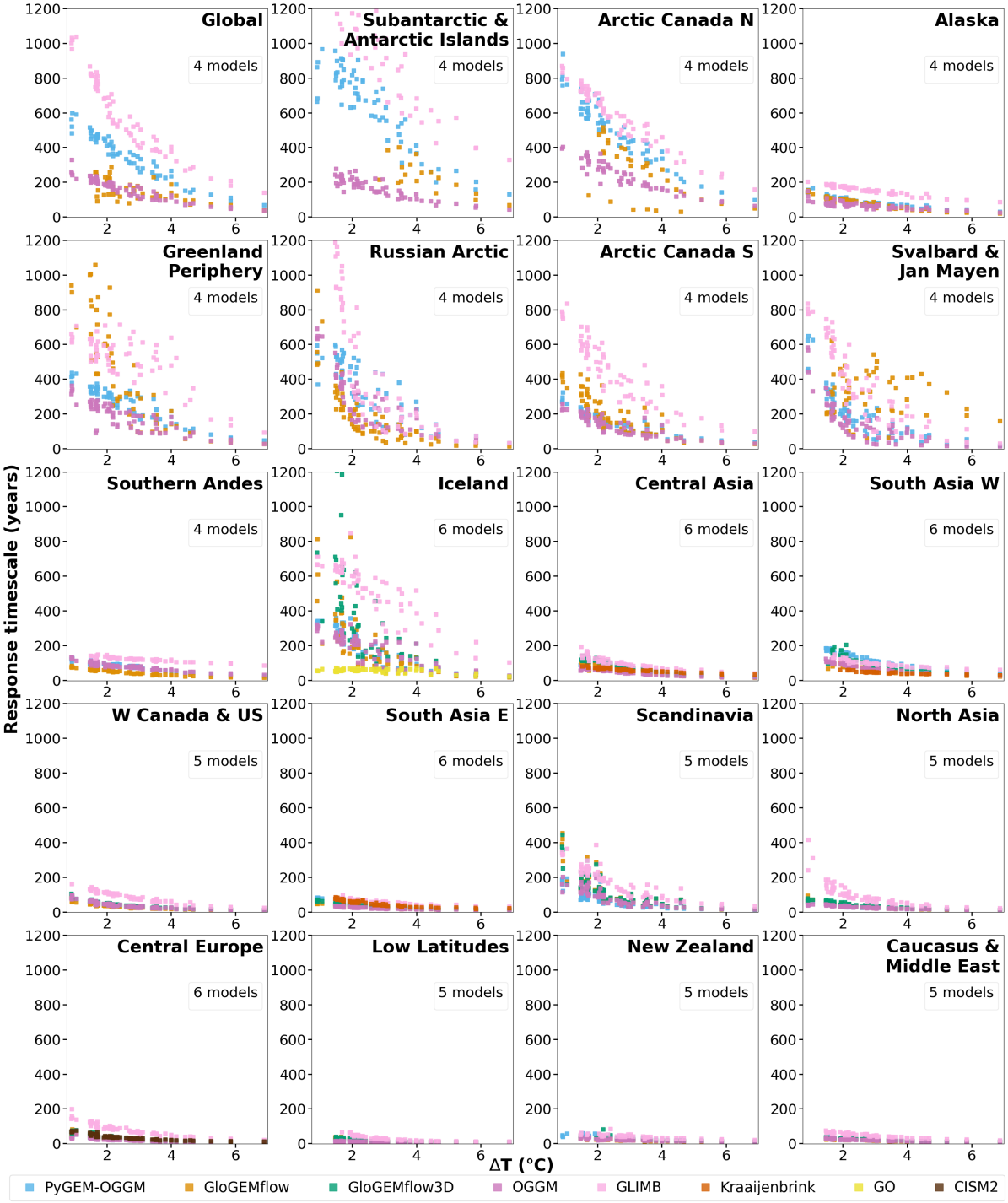

Fig. S 11. Response timescale in years from the simulation start when 80% of the committed mass loss between 2020 and steady state has occurred. Years are estimated from 21-year mass averages. Results are shown for glacier models and climate scenarios with ΔT ≥0.8°C and at least 25% of committed mass change (see Methods). For better readability, the y-axis is limited to 1200 years, which comprises 99.3% of data (a few longer response timescales exist in RGI regions 04, 05, 06, 09 and 19). Fig. S 15 shows response timescale when 50% of the committed mass change occurs.

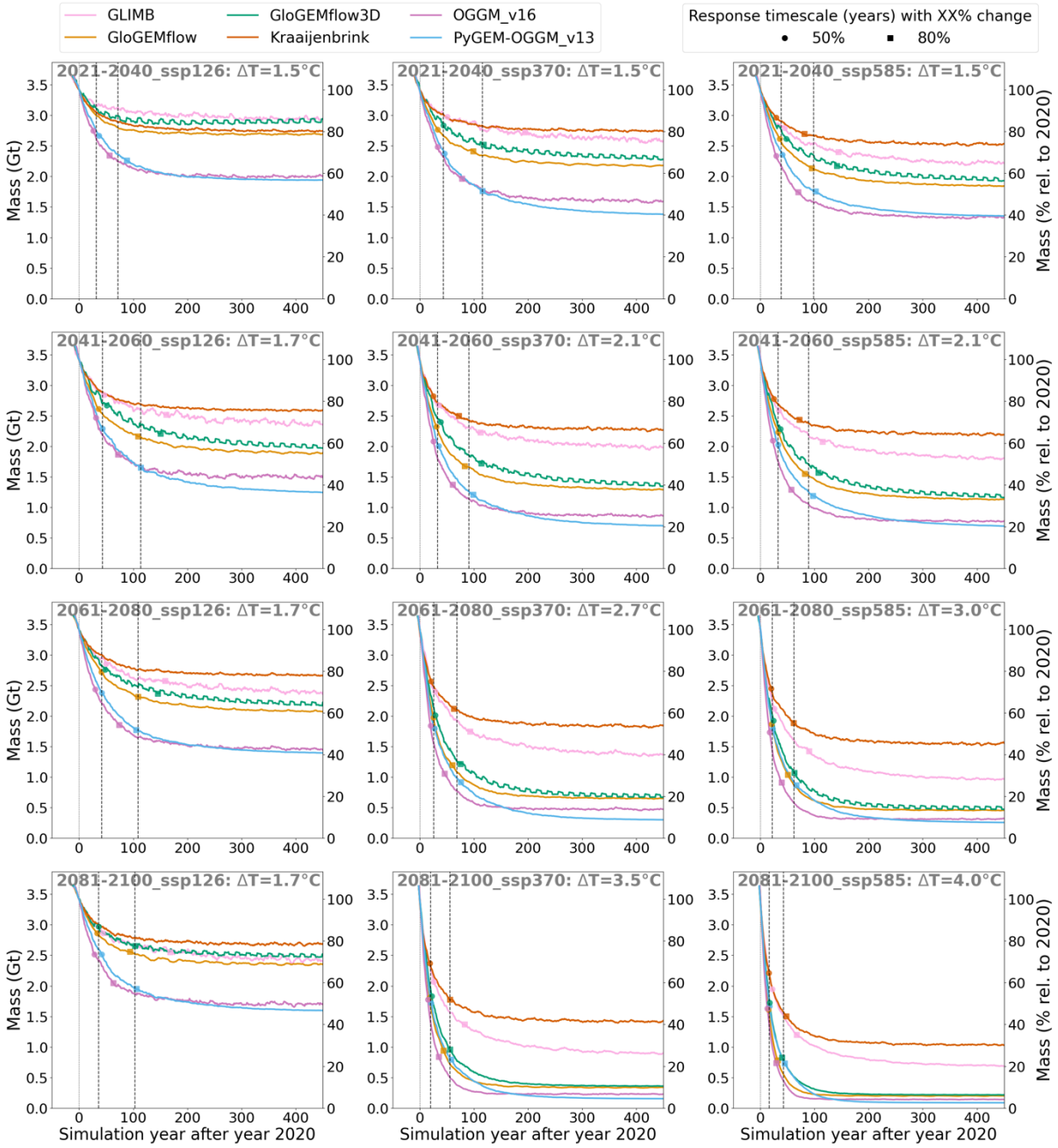

Fig. S 12. Example of regional glacier mass evolution for Central Asia (RGI region 13). Shown for all climate scenarios above ΔT=1.2°C for the MPI-ESM1-2-HR climate model, over 400 simulation years after the year 2020. For every climate scenario (panel) and glacier model (colored lines within panel), a shift occurs to the estimated 2020 mass as a starting point (see Methods). Vertical lines indicate the median values of the year to reach 50% and 80% of the total change ('response timescales', Fig. S 11 and Fig. S 15) for all climate scenarios and glacier models with at least 25% changes relative to 2020 mass. The cyclicity that appears at the end of certain simulations (here for GloGEMflow3D) results from the extension of the time series that was performed internally (Table S 2). Additional figures for other regions and climate models are available in the GitHub repository (https://github.com/GlacierMIP/GlacierMIP3) (*39*).

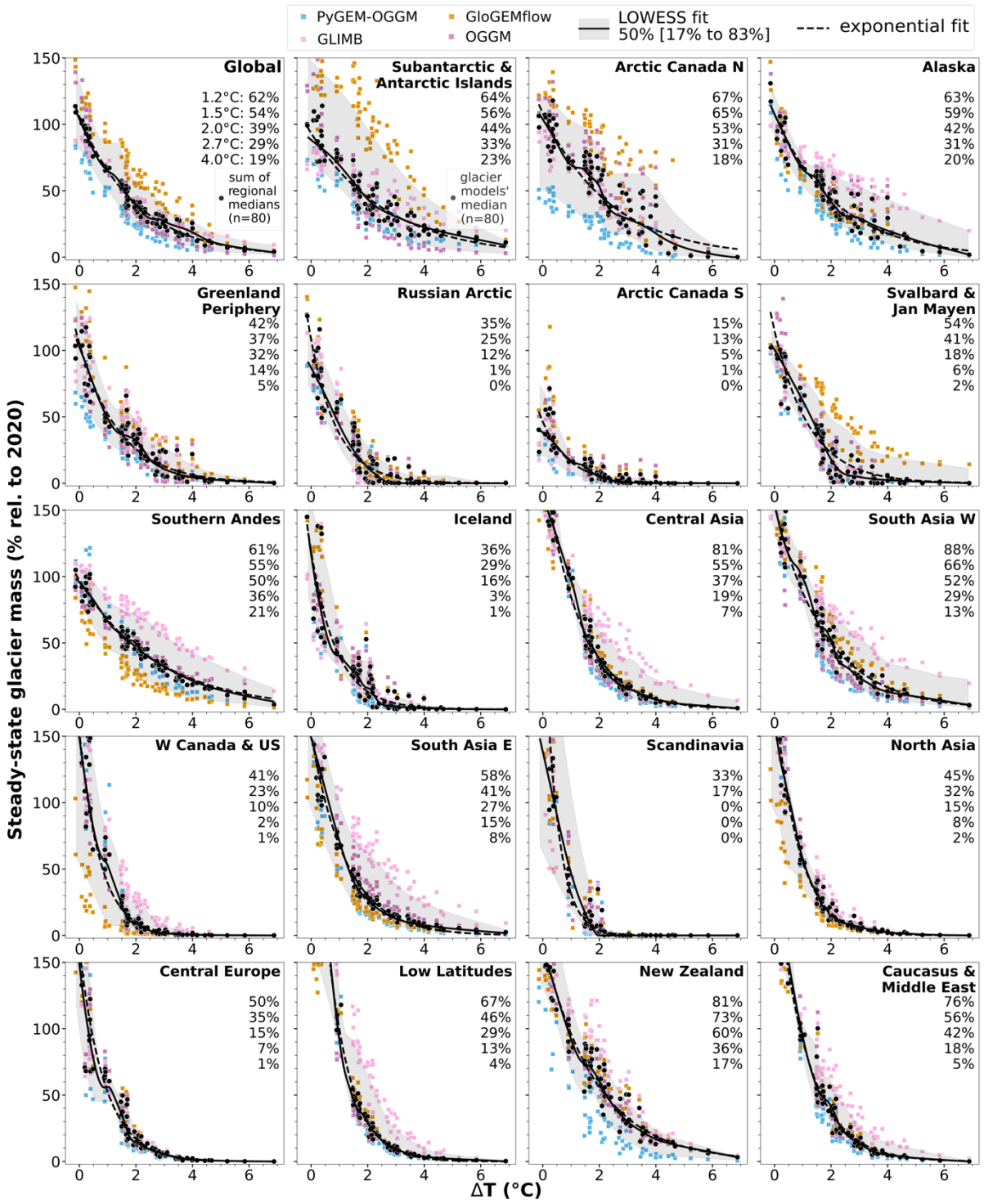

Fig. S 13. Steady-state glacier masses relative to present day (year 2020) as a function of global warming levels above pre-industrial (ΔT), when only accounting for the four global glacier models (vs. Fig. 1A and Fig. 2, which rely on data from eight glacier models). The global fit is directly performed over the global estimates, thus the percentiles are not regionally aggregated. Dots represent individual simulations forced by 80 climate scenarios per glacier model (4 glacier models per region, color-coded). Regions are sorted by descending present-day (2020) glacier mass. Numbers in the subplots are the steady state glacier masses in percent relative to present-day for distinct warming levels (see 'Global' panel for the warming levels).

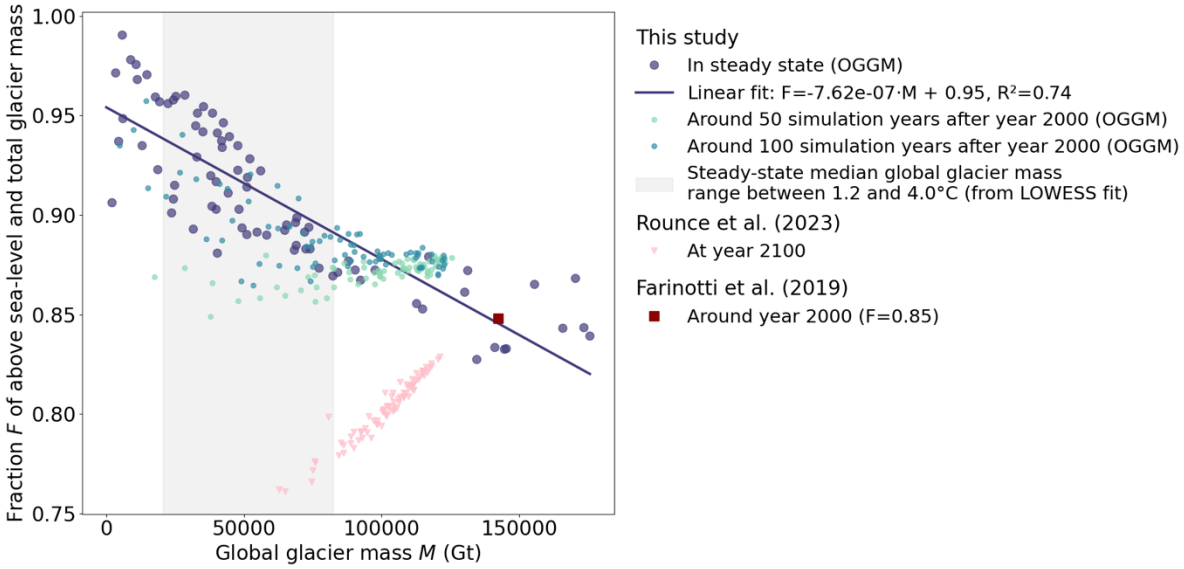

Fig. S 14. Fraction (*F*) of global above sea-level glacier mass and total glacier mass. OGGM results (this study) are shown for steady-state glacier mass and for mass after 50 or 100 simulation years. The linear fit based on the steady-state OGGM estimates was used to compute F (see legend). For comparison, the data from Rounce et al. (*10*), based on projected global glacier mass in 2100 in response to various transient climate scenarios, and the estimate by Farinotti et al. (*37*), referring to the RGI 6.0 inventory date (centered around year 2000), are also shown. The negative correlation between mass loss and remaining mass (this study, OGGM) is consistent with marine-terminating glaciers retreating gradually onto land. The contrasting positive correlation for the data by Rounce et al. (*10*) indicates that in their model, the relative depletion of submarine ice lags that of land ice.

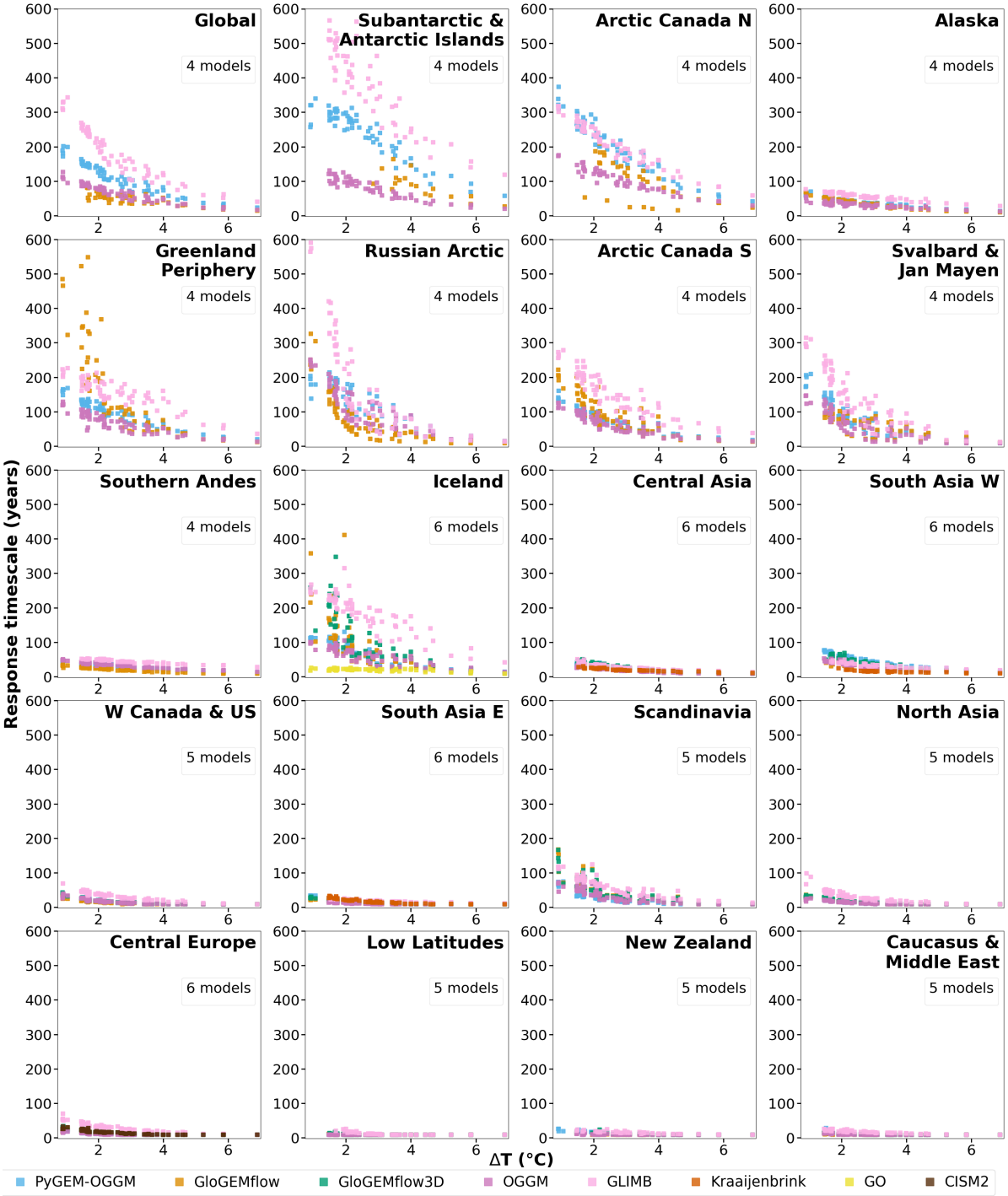

Fig. S 15. Response timescale in years from the simulation start when 50% of the committed mass loss between 2020 and steady state has occurred. Years are estimated from 21-year mass averages. Results are shown for glacier models and climate scenarios for ΔT ≥0.8°C with at least 25% of committed mass change (see Methods). For better readability, the y-axis is limited to 600 years, which comprises 99.8% of data (a few longer response timescales exist in RGI regions 05 and 19).

A Mass

	Mass 2020	Committed glacier mass loss at ΔT (% rel. to 2020)						Sensitivity (% per 0.1°C rel. to 2020)	Response timescale (years)
	(Gt)	1.2°C	1.5°C	2.0°C	2.7°C	3.0°C	4.0°C	1.5–3.0°C	1.5±0.2°C
Arctic Canada S	7212	85 [83–94]	87 [83–96]	95 [90– 98]	99 [96–100]	99 [96–100]	100 [98–100]	0.8 [0.4–1.0]	241 [190– 573]
W Canada & US	795	74 [43–93]	81 [61–94]	93 [79– 99]	98 [92– 99]	99 [94–100]	100 [98–100]	1.2 [0.4–1.6]	57 [44– 109]
Scandinavia	237	66 [24–85]	82 [51–93]	100 [83–100]	100 [100–100]	100 [100–100]	100 [100–100]	1.2 [0.8–1.5]	166 [102– 235]
Russian Arctic	12965	65 [46–80]	75 [57–89]	88 [72– 99]	99 [86–100]	100 [90–100]	100 [94–100]	1.7 [1.5–2.1]	445 [321– 902]
Iceland	3194	61 [39–73]	65 [40–80]	77 [49– 91]	96 [82– 99]	97 [83–100]	99 [92–100]	2.2 [1.4–2.6]	316 [207– 640]
Greenland Periphery	13410	58 [42–72]	63 [44–75]	68 [53– 79]	86 [70– 93]	89 [73– 96]	95 [87– 99]	1.7 [1.3–2.2]	373 [260– 656]
Central Europe	85	56 [52–61]	65 [56–75]	86 [79– 91]	93 [90– 95]	95 [93– 97]	99 [98– 99]	2.0 [1.5–2.0]	42 [29– 64]
North Asia	109	56 [46–72]	70 [58–79]	86 [79– 91]	93 [89– 95]	94 [91– 96]	98 [96– 98]	1.6 [1.2–2.0]	47 [38– 114]
South Asia E	656	49 [18–63]	63 [34–74]	74 [56– 85]	84 [62– 91]	88 [68– 93]	93 [79– 97]	1.7 [1.4–2.1]	47 [32– 72]
Svalbard & Jan Mayen	6566	46 [25–61]	59 [34–73]	82 [51– 96]	94 [63–100]	95 [70–100]	98 [79–100]	2.4 [2.1–2.4]	318 [208– 629]
Southern Andes	4368	39 [21–57]	45 [25–61]	50 [29– 73]	64 [39– 81]	68 [45– 84]	79 [57– 91]	1.5 [1.3–1.6]	86 [61– 111]
Alaska	16246	37 [30–51]	41 [31–58]	58 [34– 69]	69 [44– 79]	71 [47– 82]	80 [56– 90]	2.0 [1.3–2.1]	104 [74– 173]
Sub- & Antarctic Islands	41377	36 [-21–52]	44 [-12–59]	56 [4– 70]	67 [24– 81]	70 [31– 85]	77 [54– 91]	1.7 [1.4–2.5]	828 [224–1322]
Arctic Canada N	24851	33 [-1–67]	35 [4–70]	47 [18– 71]	69 [37– 83]	71 [37– 83]	82 [47– 95]	2.4 [1.8–2.3]	644 [356– 735]
Low Latitudes	69	23 [-8–37]	46 [13–62]	68 [47– 78]	87 [71– 90]	91 [81– 93]	96 [93– 98]	3.0 [2.1–3.7]	23 [14– 30]
Caucasus & Middle East	43	23 [15–35]	45 [18–56]	59 [43– 72]	82 [68– 87]	87 [76– 90]	95 [87– 96]	2.8 [2.3–2.7]	30 [26– 56]
New Zealand	53	15 [2–39]	24 [6–45]	34 [14– 55]	61 [46– 77]	67 [52– 80]	82 [76– 92]	2.9 [2.7–2.9]	36 [28– 45]
Central Asia	2771	12 [3–32]	35 [18–54]	57 [34– 73]	77 [48– 86]	80 [52– 89]	91 [70– 96]	3.0 [2.2–3.2]	103 [72– 138]
South Asia W	2485	5 [0–30]	17 [10–51]	38 [24– 67]	59 [36– 79]	68 [40– 84]	80 [54– 91]	3.4 [2.0–3.6]	139 [100– 175]
Global	137491	39 [15–55]	47 [20–64]	63 [43– 76]	76 [54– 82]	77 [60– 85]	86 [74– 93]	2.0 [1.6–2.4]	463 [216– 805]

B SLE

	Committed glacier mass loss at ΔT (mm SLE rel. to 2020)						Sensitivity (mm SLE per 0.1°C rel. to 2020)
	1.2°C	1.5°C	2.0°C	2.7°C	3.0°C	4.0°C	1.5–3.0°C
Global (below sea-level correction applied)	113 [43–204]	138 [59–237]	190 [128–279]	230 [159–302]	236 [178–313]	263 [218–342]	6.5 [4.6–8.9]
Global (no below sea-level correction)	144 [54–204]	174 [74–237]	234 [160–279]	279 [199–302]	286 [223–313]	316 [272–342]	7.5 [5.7–8.9]

Table S 1. Global and regional committed glacier mass losses at different warming levels, sensitivity to global mean temperature change, and response timescales. (**A**) Mass losses are shown in percent, and (**B**) globally also in sea-level equivalent (SLE), relative to the masses in 2020. Median values are provided, with the likely range (17th and 83rd percentile) in brackets, calculated from LOWESS fits (see Methods). Regions in (A) are ordered by decreasing regional relative mass loss at 1.2°C. Colors highlight the mass losses in five 20 % bins between 0 to 100%.

	CISM2	GLIMB	GloGEMflow	GloGEMflow3D	GO	Kraaijenbrink	OGGM v1.6.0	PyGEM-OGGM v1.3
Domain	RGI region 11 (Central Europe) excluding the 35 glaciers in the Pyrenees and Montenegro/Albania (ca. 0.15% of regional area). No upscaling	All RGI regions. No upscaling	All RGI regions (glaciers > 1 km^2). Upscaling of smaller glaciers to match regional volume by Farinotti et al. *(37)*	RGI regions 8, 10, 11, 12, 16, 18 (glaciers >1 km^2) and RGI regions 2, 6, 13, 14, 15 (glaciers >2 km^2). Upscaling of smaller glaciers to match regional volume by Farinotti et al. *(37)*	RGI region 6 (Iceland). No upscaling	RGI regions 13, 14, 15 (High-Mountain Asia, glaciers >0.4 km2). Upscaling of smaller glaciers using subregion specific volume-area scaling	All RGI regions. No upscaling.	All RGI regions. No upscaling.
Spatial representation	100x100m grid	0.5° x 0.5° grid	Per glacier	Per glacier	Per glacier	Per glacier	Per glacier	Per glacier
Initial glacier area / volume	Spin up using 1979–1988 climate and RGI6.0 area, until quasi-steady state is reached and then transient run forward aiming to match ice thickness fields by Farinotti et al. (*37*)	Areas from RGI6.0 and volumes by volume-area scaling tuned to match regional volumes by Farinotti et al. (*37*)	Spin up with glaciers until steady state is reached and then transiently run forward aiming to match the RGI6.0 area and glacier-specific volumes by Farinotti et al. *(37)*	Areas from RGI6.0 and volumes from ice-thickness fields by Farinotti et al. (*37*)	Areas from RGI6.0 and volumes by volume-area scaling tuned to match glacier-specific volumes by Farinotti et al. (*37*)	Area from RGI6.0 and volume from ice-thickness fields by Farinotti et al. (*37*)	Areas from RGI6.0 and volumes from ice thickness inversion tuned to match regional volumes by Farinotti et al. *(37)*.	Areas from RGI6.0 and volumes from ice thickness inversion tuned to match regional volumes by Farinotti et al. (*37*) based on land-terminating glaciers only (thus volume changes when frontal ablation is included).
Meteorological forcing data for calibration	Monthly temperature and precipitation from W5E5 v2.0 *(51)*	Daily temperature, precipitation, relative humidity, wind speed, and downward solar radiation, from ERA5 *(52)*	Monthly temperature and precipitation from ERA5 *(52)*	Monthly temperature and precipitation from ERA5 *(52)*	Monthly temperature and precipitation from ERA5 *(52)*. Transformed to daily values by linearly interpolating temperature and repeating precipitation for each day in a month	Monthly temperature and precipitation from W5E5 v2.0 *(51)*	Monthly temperature and precipitation from W5E5 v2.0 *(51)*	Monthly temperature and precipitation from ERA5 *(52)*
Climatic MB	Melt from PDD (1 DDF), accumulation from precipitation below threshold temperature, snow accumulation set to zero outside the RGI extent to reduce spurious glacier advance	Melt from Energy balance, accumulation from precipitation below temperature threshold, refreezing accounted for	Melt from PDD (2 DDFs), accumulation from precipitation below temperature threshold, refreezing accounted for	Melt from PDD (2 DDFs), accumulation from precipitation below temperature threshold, refreezing accounted for	Melt from simplified energy balance, accumulation from precipitation below temperature threshold, refreezing accounted for	Imposed elevation-dependent MB gradient, with maximum ablation limited by PDD and terminus DDF, maximum accumulation limited by annual precipitation. Modulation of MB for each bin using parameterized debris thickness and supraglacial pond area	Melt from PDD (1 DDF), accumulation from precipitation below temperature threshold	Melt from PDD, 2 DDFs + debris melt enhancement factor; accumulation from precipitation below temperature threshold, refreezing accounted for
Other MB components	Basal melt beneath grounded ice when at pressure melting point	-	Parameterized frontal ablation, as in *(53)*	-	-	-	-	Parameterized frontal ablation
MB calibration data and method	Per-glacier calibration based on geodetic MB *(1)* averaged over Jan 2000–Dec 2019 and assuming zero MB over period 1979–1988. Calibration through DDF and precipitation correction factor. Added a temperature bias when the above two parameters fall outside a user-defined range	Gridded calibration based on geodetic MB *(1)* averaged over Jan 2000–Dec 2019 at 0.5° x 0.5° resolution. Calibration through precipitation correction factor. Added a temperature bias when the precipitation correction factor is outside the 0.05 to 20 range	Per-glacier calibration based on geodetic MB *(1)* averaged over Jan 2000-Dec 2019. Various frontal ablation calibration datasets, same as used in *(53)* Calibration as in Zekollari et al. (*11*), where a DDF and precipitation correction factor are adapted. Added a temperature bias when the above two parameters fall outside a user-defined range	Per-glacier calibration based on geodetic MB *(1)* averaged over Jan 2000-Dec 2019. Various frontal ablation calibration datasets, same as used in *(53)* Calibration as in Zekollari et al. (*11*), where a DDF and precipitation correction factor are adapted. Added a temperature bias when the above two parameters fall outside a user-defined range	Per-glacier calibration based on geodetic MB *(1)* averaged over Jan 2000–Dec 2019. Calibration of seven parameters for ensemble of 250 combinations. Optimal parameter set selected for each glacier minimizing the RMSE between modelled and observed MB	Per-glacier calibration based on geodetic MB *(54)* averaged over Jun 2000–Jun 2018, surface area in each elevation band, and degree days at terminus Calibrated as in Kraaijenbrink et al. *(55)*, where MB gradient per glacier is adapted	Per-glacier calibration based on geodetic MB *(1)* averaged over Jan 2000–Dec 2019. Winter MB observations *(56)* used to compute a winter-precipitation dependent precipitation correction factor. Calibration as in Zekollari et al. *(11)*, but assuming fixed glacier geometry, where a precipitation correction factor, temperature bias, and DDF are adapted	Per-glacier calibration based on geodetic MB *(1)* averaged over Jan 2000–Dec 2019. Winter MB observations *(56)* indirectly used to set limits of precipitation factor for prior distributions for calibration. Various frontal ablation calibration datasets, same as used in *(10)* Calibration as in Rounce et al. *(10)* through Bayesian inference assuming fixed geometry, where DDF, precipitation correction factor, and

								temperature bias are calibrated
Bias correction period and approach	Matched climate model data to W5E5v2.0 (*51*) over period 1979–2014 by using quantile mapping (applied directly bias-corrected climate models from ISIMIP3b (*57*)	Matched climate model data to ERA5 (*52*) over period 2000–2020 by correcting for mean temperature (additive), temperature variability (multiplicative), and precipitation (multiplicative)	Matched climate model data to ERA5 (*52*) over period 1980–2019 by correcting for mean temperature (additive), temperature variability (multiplicative), and precipitation (multiplicative) (*53*)	Matched climate model data to ERA5 (*52*) over period 1980–2019 by correcting for mean temperature (additive), temperature variability (multiplicative), and precipitation (multiplicative) (*53*)	Matched climate model data to ERA5 (*52*) over period 1980–2019 by correcting for mean temperature (additive) and precipitation (multiplicative)	Matched climate model data to W5E5v2.0 (*51*) over period 1991–2014 by correcting for mean temperature (additive) and precipitation (multiplicative)	Matched climate model data to W5E5v2.0 (*51*) over period 1979–2014 by using quantile mapping (applied directly bias-corrected climate models from ISIMIP3b (*57*)	Matched climate model data to ERA5 (*52*) over period 2000–2019 by correcting for mean temperature (additive), temperature variability (multiplicative), and precipitation (multiplicative) (*53*)
Geometry changes	3D ice flow model (depth-integrated higher-order velocity solver), 100 m grid resolution, geometry updated monthly	Volume-area scaling (hypsometry adjusted using simple geometric model at 50 m vertical resolution), geometry updated annually	1D flowline model (Shallow Ice Approximation), 100 horizontally equidistant grid points along flowline, geometry updated at least annually	Ice geometry in 3D with 2D ice flow model (Shallow Ice Approximation), resolution depending on area at initialization: 50 m (<5 km^2), 100 m (5–20 km^2), 150 m (20–100 km^2), 250 m (100–500 km^2), 500 m (>500 km^2), geometry updated at least annually	Volume-area scaling, geometry updated annually	Simplified volume-area relation of each specific elevation bin, geometry updated annually	1D flowline model (Shallow Ice Approximation), horizontally equidistant grid points along flowline, 20–400 m resolution, geometry updated annually	1D flowline model (Shallow Ice Approximation), horizontally equidistant grid points along flowline, geometry updated annually; for cases where flowline model failed (some tidewater glaciers): used mass redistribution curves (*58*) instead
Simulation period	2000 years	2000/5000 years depending on region	Each glacier's simulation stopped when 100-year mean specific MB was within ±9 kg m^{-2} $year^{-1}$. Time series duration extended to 2000/5000 years by repeatedly appending the data from the last 50 years.	Each glacier's simulation stopped when 100-year mean specific MB was within ±2 kg m^{-2} $year^{-1}$. Time series duration extended to 2000/5000 years by repeatedly appending the data from the last 20 years.	5000 years	2000 years	2000/5000 years depending on region	Each glacier's simulation stopped when volume was 0 (over at least 20 years) or 100-year mean specific MB was within ±10 kg m^{-2} $year^{-1}$. Time series duration extended to 2000/5000 years by repeatedly appending the data from the last 20 years.
Reference and other notes	CISM2 (*59*) was developed for ice sheets, first use as regional glacier model by using similar settings as for ice sheets but adjustments for surface MB calibration, glacier-tracking logic, and parameters	Original GLIMB study *(60)*. Precipitation calibration *(61)*. Application to HMA glaciers *(62)*	Extended version of GloGEM *(53)*, to include ice dynamics *(63, 64)*	Extended version of GloGEMflow to account for 3D glacier geometry	Rewritten version of the model by Giesen and Oerlemans *(65)*	Kraaijenbrink et al. *(55)*	Model description: Maussion et al. *(49)*; Version used here: Maussion et al. *(66)*	Rounce et al. *(10)*

Table S 2. Glacier model characteristics. Abbreviations: DDF: Degree-day Factor, MB: mass balance, PDD: Positive Degree-Day model.

	Year[a]	Glacier area[b] (km²)	Glacier surface slope[b] (glacier-area weighted average, °)	Glacier mass[b] (Gt)	Glacier mass in 2020[c] (Gt)	2000–2019 observed glacier mass loss[c] (rel. to 2000, %)	Simulation time (years)
Global	2000	705739	11.4	142341	137491	3.9	
Sub- & Antarctic Islands (19)	1986	132867	3.6	41820	41377	1.1	5000
Arctic Canada N (03)	1999	105111	9.6	25498	24851	2.5	5000
Alaska (01)	2010	86725	13.9	17081	16246	8.0	5000
Greenland Periphery (05)	2001	89717	10.3	14123	13410	5.3	5000
Russian Arctic (09)	2001	51592	11.9	13176	12965	1.7	5000
Arctic Canada S (04)	2001	40888	11.5	7750	7212	7.2	5000
Svalbard (07)	2008	33959	8.8	6723	6566	3.3	5000
Southern Andes (17)	2000	29429	14.9	4806	4368	9.1	5000
Iceland (06)	2000	11060	6.7	3393	3194	5.8	5000
Central Asia (13)	2007	49303	19.5	2944	2771	6.8	2000
South Asia W (14)	2001	33568	22.3	2579	2485	3.7	2000
W Canada & US (02)	2004	14524	18.3	942	795	16.8	2000
South Asia E (15)	2002	14734	21.1	790	656	18.2	2000
Scandinavia (08)	2002	2949	11.9	269	237	12.9	2000
North Asia (10)	2011	2410	18.4	122	109	19.6	2000
Central Europe (11)	2003	2092	20.9	115	85	29.7	2000
Low Latitudes (16)	2000	2341	25.3	89	69	22.3	2000
New Zealand (18)	1978	1162	25.6	66	53	20.8	2000
Caucasus & Middle East (12)	2001	1307	24.2	57	43	25.0	2000

Table S 3. Regional past or current glacier characteristics and simulation time years. Regions (with RGI6.0 region numbers in brackets) are sorted after glacier mass in 2020. a: refers to the year of the median area-weighted RGI-year of all glaciers in a region, yr_{RGI} (*40*), b: Estimates refer to the year given in column "Year", c: Estimates from Farinotti et al. (*37*) (around year 2000) reprojected to 2020 based on mass change data from Hugonnet et al. (*1*) (see Methods).

References and Notes

1. R. Hugonnet, R. McNabb, E. Berthier, B. Menounos, C. Nuth, L. Girod, D. Farinotti, M. Huss, I. Dussaillant, F. Brun, A. Kääb, Accelerated global glacier mass loss in the early twenty-first century. *Nature* **592**, 726–731 (2021). doi:10.1038/s41586-021-03436-z Medline

2. T. L. Edwards, S. Nowicki, B. Marzeion, R. Hock, H. Goelzer, H. Seroussi, N. C. Jourdain, D. A. Slater, F. E. Turner, C. J. Smith, C. M. McKenna, E. Simon, A. Abe-Ouchi, J. M. Gregory, E. Larour, W. H. Lipscomb, A. J. Payne, A. Shepherd, C. Agosta, P. Alexander, T. Albrecht, B. Anderson, X. Asay-Davis, A. Aschwanden, A. Barthel, A. Bliss, R. Calov, C. Chambers, N. Champollion, Y. Choi, R. Cullather, J. Cuzzone, C. Dumas, D. Felikson, X. Fettweis, K. Fujita, B. K. Galton-Fenzi, R. Gladstone, N. R. Golledge, R. Greve, T. Hattermann, M. J. Hoffman, A. Humbert, M. Huss, P. Huybrechts, W. Immerzeel, T. Kleiner, P. Kraaijenbrink, S. Le Clec'h, V. Lee, G. R. Leguy, C. M. Little, D. P. Lowry, J.-H. Malles, D. F. Martin, F. Maussion, M. Morlighem, J. F. O'Neill, I. Nias, F. Pattyn, T. Pelle, S. F. Price, A. Quiquet, V. Radić, R. Reese, D. R. Rounce, M. Rückamp, A. Sakai, C. Shafer, N.-J. Schlegel, S. Shannon, R. S. Smith, F. Straneo, S. Sun, L. Tarasov, L. D. Trusel, J. Van Breedam, R. van de Wal, M. van den Broeke, R. Winkelmann, H. Zekollari, C. Zhao, T. Zhang, T. Zwinger, Projected land ice contributions to twenty-first-century sea level rise. *Nature* **593**, 74–82 (2021). doi:10.1038/s41586-021-03302-y Medline

3. L. Jakob, N. Gourmelen, Glacier mass loss between 2010 and 2020 dominated by atmospheric forcing. *Geophys. Res. Lett.* **50**, e2023GL102954 (2023). doi:10.1029/2023GL102954

4. M. Huss, R. Hock, Global-scale hydrological response to future glacier mass loss. *Nat. Clim. Chang.* **8**, 135–140 (2018). doi:10.1038/s41558-017-0049-x

5. J. B. Bosson, M. Huss, S. Cauvy-Fraunié, J. C. Clément, G. Costes, M. Fischer, J. Poulenard, F. Arthaud, Future emergence of new ecosystems caused by glacial retreat. *Nature* **620**, 562–569 (2023). doi:10.1038/s41586-023-06302-2 Medline

6. Y. Ding, C. Mu, T. Wu, G. Hu, D. Zou, D. Wang, W. Li, X. Wu, Increasing cryospheric hazards in a warming climate. *Earth Sci. Rev.* **213**, 103500 (2021). doi:10.1016/j.earscirev.2020.103500

7. E. Salim, Glacier tourism without ice: Envisioning future adaptations in a melting world. *Front. Hum. Dyn.* **5**, 1137551 (2023). doi:10.3389/fhumd.2023.1137551

8. R. Hock, A. Bliss, B. Marzeion, R. H. Giesen, Y. Hirabayashi, M. Huss, V. Radić, A. B. A. Slangen, GlacierMIP – A model intercomparison of global-scale glacier mass-balance models and projections. *J. Glaciol.* **65**, 453–467 (2019). doi:10.1017/jog.2019.22

9. B. Marzeion, R. Hock, B. Anderson, A. Bliss, N. Champollion, K. Fujita, M. Huss, W. W. Immerzeel, P. Kraaijenbrink, J.-H. Malles, F. Maussion, V. Radić, D. R. Rounce, A. Sakai, S. Shannon, R. van de Wal, H. Zekollari, Partitioning the uncertainty of ensemble projections of global glacier mass change. *Earths Futur.* **8**, e2019EF001470 (2020). doi:10.1029/2019EF001470

10. D. R. Rounce, R. Hock, F. Maussion, R. Hugonnet, W. Kochtitzky, M. Huss, E. Berthier, D. Brinkerhoff, L. Compagno, L. Copland, D. Farinotti, B. Menounos, R. W. McNabb, Global glacier change in the 21st century: Every increase in temperature matters. *Science* **379**, 78–83 (2023). doi:10.1126/science.abo1324 Medline

11. H. Zekollari, M. Huss, L. Schuster, F. Maussion, D. R. Rounce, R. Aguayo, N. Champollion, L. Compagno, R. Hugonnet, B. Marzeion, S. Mojtabavi, D. Farinotti, Twenty-first century global glacier evolution under CMIP6 scenarios and the role of glacier-specific observations. *Cryosphere* **18**, 5045–5066 (2024). doi:10.5194/tc-18-5045-2024

12. J. E. Christian, M. Koutnik, G. Roe, Committed retreat: Controls on glacier disequilibrium in a warming climate. *J. Glaciol.* **64**, 675–688 (2018). doi:10.1017/jog.2018.57

13. B. Marzeion, G. Kaser, F. Maussion, N. Champollion, Limited influence of climate change mitigation on short-term glacier mass loss. *Nat. Clim. Chang.* **8**, 305–308 (2018). doi:10.1038/s41558-018-0093-1

14. H. Zekollari, M. Huss, D. Farinotti, On the imbalance and response time of glaciers in the European Alps. *Geophys. Res. Lett.* **47**, e2019GL085578 (2020). doi:10.1029/2019GL085578

15. J. G. Cogley, R. Hock, L. A. Rasmussen, A. A. Arendt, A. Bauder, P. Jansson, R. J. Braithwaite, G. Kaser, M. Moller, L. Nicholson, M. Zemp, "Glossary of glacier mass balance and related terms" (IACS Technical Report 86, 2011); https://unesdoc.unesco.org/ark:/48223/pf0000192525.

16. T. Johannesson, C. Raymond, E. Waddington, Time-scale for adjustment of glaciers to changes in mass balance. *J. Glaciol.* **35**, 355–369 (1989). doi:10.3189/S002214300000928X

17. D. B. Bahr, W. T. Pfeffer, C. Sassolas, M. F. Meier, Response times of glaciers as a function of size and mass balance: 1. Theory. *J. Geophys. Res.* **103**, 9777–9782 (1998). doi:10.1029/98JB00507

18. M. Schäfer, M. Möller, T. Zwinger, J. C. Moore, Dynamic modelling of future glacier changes: Mass-balance/elevation feedback in projections for the Vestfonna ice cap, Nordaustlandet, Svalbard. *J. Glaciol.* **61**, 1121–1136 (2015). doi:10.3189/2015JoG14J184

19. E. Johnson, S. Rupper, An examination of physical processes that trigger the albedo-feedback on glacier surfaces and implications for regional glacier mass balance across high mountain Asia. *Front. Earth Sci. (Lausanne)* **8**, 8 (2020). doi:10.3389/feart.2020.00129

20. G. H. Roe, M. B. Baker, F. Herla, Centennial glacier retreat as categorical evidence of regional climate change. *Nat. Geosci.* **10**, 95–99 (2017). doi:10.1038/ngeo2863

21. A. Huston, N. Siler, G. H. Roe, E. Pettit, N. J. Steiger, Understanding drivers of glacier-length variability over the last millennium. *Cryosphere* **15**, 1645–1662 (2021). doi:10.5194/tc-15-1645-2021

22. O. N. Solomina, R. S. Bradley, V. Jomelli, A. Geirsdottir, D. S. Kaufman, J. Koch, N. P. McKay, M. Masiokas, G. Miller, A. Nesje, K. Nicolussi, L. A. Owen, A. E. Putnam, H. Wanner, G. Wiles, B. Yang, Glacier fluctuations during the past 2000 years. *Quat. Sci. Rev.* **149**, 61–90 (2016). doi:10.1016/j.quascirev.2016.04.008

23. S. H. Mernild, W. H. Lipscomb, D. B. Bahr, V. Radić, M. Zemp, Global glacier changes: A revised assessment of committed mass losses and sampling uncertainties. *Cryosphere* **7**, 1565–1577 (2013). doi:10.5194/tc-7-1565-2013

24. P. M. Forster, C. Smith, T. Walsh, W. F. Lamb, R. Lamboll, B. Hall, M. Hauser, A. Ribes, D. Rosen, N. P. Gillett, M. D. Palmer, J. Rogelj, K. von Schuckmann, B. Trewin, M. Allen, R. Andrew, R. A. Betts, A. Borger, T. Boyer, J. A. Broersma, C. Buontempo, S. Burgess, C. Cagnazzo, L. Cheng, P. Friedlingstein, A. Gettelman, J. Gütschow, M. Ishii, S. Jenkins, X. Lan, C. Morice, J. Mühle, C. Kadow, J. Kennedy, R. E. Killick, P. B. Krummel, J. C. Minx, G. Myhre, V. Naik, G. P. Peters, A. Pirani, J. Pongratz, C.-F. Schleussner, S. I. Seneviratne, S. Szopa, P. Thorne, M. V. M. Kovilakam, E. Majamäki, J.-P. Jalkanen, M. van Marle, R. M. Hoesly, R. Rohde, D. Schumacher, G. van der Werf, R. Vose, K. Zickfeld, X. Zhang, V. Masson-Delmotte, P. Zhai, Indicators of Global Climate Change 2023: Annual update of key indicators of the state of the climate system and human influence. *Earth Syst. Sci. Data* **16**, 2625–2658 (2024). doi:10.5194/essd-16-2625-2024

25. International Panel on Climate Change, "Climate change 2021: The physical science basis. Contribution of Working Group I to the sixth assessment report of the Intergovernmental Panel on Climate Change" (IPCC, 2021); https://www.ipcc.ch/report/ar6/wg1/.

26. Mountain Research Initiative EDW Working Group, Elevation-dependent warming in mountain regions of the world. *Nat. Clim. Change* **5**, 424–430 (2015). doi:10.1038/nclimate2563

27. D. M. Smith, J. A. Screen, C. Deser, J. Cohen, J. C. Fyfe, J. García-Serrano, T. Jung, V. Kattsov, D. Matei, R. Msadek, Y. Peings, M. Sigmond, J. Ukita, J.-H. Yoon, X. Zhang, The Polar Amplification Model Intercomparison Project (PAMIP) contribution to CMIP6: Investigating the causes and consequences of polar amplification. *Geosci. Model Dev.* **12**, 1139–1164 (2019). doi:10.5194/gmd-12-1139-2019

28. A. Gardner, G. Moholdt, A. Arendt, B. Wouters, Accelerated contributions of Canada's Baffin and Bylot Island glaciers to sea level rise over the past half century. *Cryosphere* **6**, 1103–1125 (2012). doi:10.5194/tc-6-1103-2012

29. A. Gilbert, G. E. Flowers, G. H. Miller, B. T. Rabus, W. Van Wychen, A. S. Gardner, L. Copland, Sensitivity of Barnes Ice Cap, Baffin Island, Canada, to climate state and internal dynamics. *J. Geophys. Res. Earth Surf.* **121**, 1516–1539 (2016). doi:10.1002/2016JF003839

30. Climate Action Tracker, "The CAT Thermometer" (CAT, 2023); https://climateactiontracker.org/global/cat-thermometer.

31. D. Parkes, B. Marzeion, Twentieth-century contribution to sea-level rise from uncharted glaciers. *Nature* **563**, 551–554 (2018). doi:10.1038/s41586-018-0687-9 Medline

32. D. Parkes, H. Goosse, Modelling regional glacier length changes over the last millennium using the Open Global Glacier Model. *Cryosphere* **14**, 3135–3153 (2020). doi:10.5194/tc-14-3135-2020

33. F. Paul, T. Bolch, "Glacier changes since the Little Ice Age" in *Geomorphology of Proglacial Systems*, T. Heckmann, D. Morche, Eds. (Springer, 2019), pp. 23–42.

34. G. Roe, J. E. Christian, B. Marzeion, On the attribution of industrial-era glacier mass loss to anthropogenic climate change. *Cryosphere* **15**, 1889–1905 (2021). doi:10.5194/tc-15-1889-2021

35. B. Marzeion, J. G. Cogley, K. Richter, D. Parkes, Glaciers. Attribution of global glacier mass loss to anthropogenic and natural causes. *Science* **345**, 919–921 (2014). doi:10.1126/science.1254702 Medline

36. United Nations, "International year of glaciers' preservation, 2025: revised draft resolution" (UN, 2022); https://digitallibrary.un.org/record/3994297.

37. D. Farinotti, M. Huss, J. J. Fürst, J. Landmann, H. Machguth, F. Maussion, A. Pandit, A consensus estimate for the ice thickness distribution of all glaciers on Earth. *Nat. Geosci.* **12**, 168–173 (2019). doi:10.1038/s41561-019-0300-3

38. Data for: H. Zekollari, L. Schuster, F. Maussion, R. Hock, B. Marzeion, D. R. Rounce, L. Compagno, K. Fujita, M. Huss, M. James, P. D. A. Kraaijenbrink, W. H. Lipscomb, S. Minallah, M. Oberrauch, L. Van Tricht, N. Champollion, T. Edwards, D. Farinotti, W. Immerzeel, G. Leguy, A. Sakai, Glacier preservation doubled by limiting warming to 1.5°C versus 2.7°C, Zenodo (2024); https://doi.org/10.5281/zenodo.14045268.

39. Code for: H. Zekollari, L. Schuster, F. Maussion, R. Hock, B. Marzeion, D. R. Rounce, L. Compagno, K. Fujita, M. Huss, M. James, P. D. A. Kraaijenbrink, W. H. Lipscomb, S. Minallah, M. Oberrauch, L. Van Tricht, N. Champollion, T. Edwards, D. Farinotti, W. Immerzeel, G. Leguy, A. Sakai, Glacier preservation doubled by limiting warming to 1.5°C versus 2.7°C, Zenodo (2024); https://doi.org/10.5281/zenodo.15046031.

40. Randolph Glacier Inventory Consortium, "Randolph Glacier Inventory – A Dataset of Global Glacier Outlines: Version 6.0: Technical Report, Global Land Ice Measurements from Space, Colorado, USA" (RGI, 2017); https://doi.org/10.7265/N5-RGI-60.

41. International Panel on Climate Change, "Summary for policymakers" in *IPCC Special Report on the Ocean and Cryosphere in a Changing Climate*, H.-O. Pörtner, D. C. Roberts, V. Masson-Delmotte, P. Zhai, M. Tignor, E. Poloczanska, K. Mintenbeck, M. Nicolai, A. Okem, J. Petzold, B. Rama, N. Weyer, Eds. (IPCC, 2019); https://www.ipcc.ch/srocc/chapter/summary-for-policymakers/.

42. H. Goosse, J. E. Kay, K. C. Armour, A. Bodas-Salcedo, H. Chepfer, D. Docquier, A. Jonko, P. J. Kushner, O. Lecomte, F. Massonnet, H.-S. Park, F. Pithan, G. Svensson, M. Vancoppenolle, Quantifying climate feedbacks in polar regions. *Nat. Commun.* **9**, 1919 (2018). doi:10.1038/s41467-018-04173-0 Medline

43. A. D. King, T. P. Lane, B. J. Henley, J. R. Brown, Global and regional impacts differ between transient and equilibrium warmer worlds. *Nat. Clim. Chang.* **10**, 42–47 (2020). doi:10.1038/s41558-019-0658-7

44. F. A. Ziemen, R. Hock, A. Aschwanden, C. Khroulev, C. Kienholz, A. Melkonian, J. Zhang, Modeling the evolution of the Juneau Icefield using the Parallel Ice Sheet Model (PISM). *J. Glaciol.* **62**, 199–214 (2016). doi:10.1017/jog.2016.13

45. I. Dussaillant, R. Hugonnet, M. Huss, E. Berthier, J. Bannwart, F. Paul, M. Zemp, Annual mass changes for each glacier in the world from 1976 to 2023. *Earth System Science Data* **17**, 1977–2006 (2025). doi:10.5194/essd-17-1977-2025

46. W. S. Cleveland, Robust locally weighted regression and smoothing scatterplots. *J. Am. Stat. Assoc.* **74**, 829–836 (1979). doi:10.1080/01621459.1979.10481038

47. A. Bourn, "AyrtonB/Merit-Order-Effect: v1.0.0" (2021); https://doi.org/10.5281/ZENODO.4642896.

48. P. Virtanen, R. Gommers, T. E. Oliphant, M. Haberland, T. Reddy, D. Cournapeau, E. Burovski, P. Peterson, W. Weckesser, J. Bright, S. J. van der Walt, M. Brett, J. Wilson, K. J. Millman, N. Mayorov, A. R. J. Nelson, E. Jones, R. Kern, E. Larson, C. J. Carey, İ. Polat, Y. Feng, E. W. Moore, J. VanderPlas; SciPy 1.0 Contributors, SciPy 1.0: Fundamental algorithms for scientific computing in Python. *Nat. Methods* **17**, 261–272 (2020). doi:10.1038/s41592-019-0686-2 Medline

49. F. Maussion, A. Butenko, N. Champollion, M. Dusch, J. Eis, K. Fourteau, P. Gregor, A. H. Jarosch, J. Landmann, F. Oesterle, B. Recinos, T. Rothenpieler, A. Vlug, C. T. Wild, B. Marzeion, The Open Global Glacier Model (OGGM) v1.1. *Geosci. Model Dev.* **12**, 909–931 (2019). doi:10.5194/gmd-12-909-2019

50. S. Lange, M. Mengel, S. Treu, M. Büchner, "ISIMIP3a atmospheric climate input data, version 1.2" (ISIMIP Repository, 2022); https://doi.org/10.48364/ISIMIP.982724.2.

51. S. Lange, C. Menz, S. Gleixner, M. Cucchi, G. P. Weedon, A. Amici, N. Bellouin, H. Müller Schmied, H. Hersbach, C. Buontempo, C. Cagnazzo, "WFDE5 over land merged with ERA5 over the ocean (W5E5 v2.0)" (ISIMIP Repository, 2021); https://doi.org/10.48364/ISIMIP.342217.

52. H. Hersbach, B. Bell, P. Berrisford, S. Hirahara, A. Horányi, J. Muñoz-Sabater, J. Nicolas, C. Peubey, R. Radu, D. Schepers, A. Simmons, C. Soci, S. Abdalla, X. Abellan, G. Balsamo, P. Bechtold, G. Biavati, J. Bidlot, M. Bonavita, G. De Chiara, P. Dahlgren, D. Dee, M. Diamantakis, R. Dragani, J. Flemming, R. Forbes, M. Fuentes, A. Geer, L. Haimberger, S. Healy, R. J. Hogan, E. Hólm, M. Janisková, S. Keeley, P. Laloyaux, P. Lopez, C. Lupu, G. Radnoti, P. de Rosnay, I. Rozum, F. Vamborg, S. Villaume, J.-N. Thépaut, The ERA5 global reanalysis. *Q. J. R. Meteorol. Soc.* **146**, 1999–2049 (2020). doi:10.1002/qj.3803

53. M. Huss, R. Hock, A new model for global glacier change and sea-level rise. *Front. Earth Sci.* **3**, 54 (2015).

54. D. E. Shean, S. Bhushan, P. Montesano, D. R. Rounce, A. Arendt, B. Osmanoglu, A systematic, regional assessment of high mountain asia glacier mass balance. *Front. Earth Sci.* **7**, 00363 (2020) doi:10.3389/feart.2019.00363.

55. P. D. A. Kraaijenbrink, M. F. P. Bierkens, A. F. Lutz, W. W. Immerzeel, Impact of a global temperature rise of 1.5 degrees Celsius on Asia's glaciers. *Nature* **549**, 257–260 (2017). doi:10.1038/nature23878 Medline

56. World Glacier Monitoring Service, "Global glacier change bulletin no. 4 (2018-2019)" (WGMS, 2021); https://wgms.ch/ggcb/.

57. S. Lange, Trend-preserving bias adjustment and statistical downscaling with ISIMIP3BASD (v1.0). *Geosci. Model Dev.* **12**, 3055–3070 (2019). doi:10.5194/gmd-12-3055-2019

58. M. Huss, G. Jouvet, D. Farinotti, A. Bauder, Future high-mountain hydrology: A new parameterization of glacier retreat. *Hydrol. Earth Syst. Sci.* **14**, 815–829 (2010). doi:10.5194/hess-14-815-2010

59. W. H. Lipscomb, S. F. Price, M. J. Hoffman, G. R. Leguy, A. R. Bennett, S. L. Bradley, K. J. Evans, J. G. Fyke, J. H. Kennedy, M. Perego, D. M. Ranken, W. J. Sacks, A. G. Salinger, L. J. Vargo, P. H. Worley, Description and evaluation of the Community Ice Sheet Model (CISM) v2.1. *Geosci. Model Dev.* **12**, 387–424 (2019). doi:10.5194/gmd-12-387-2019

60. K. Fujita, Y. Ageta, Effect of summer accumulation on glacier mass balance on the Tibetan Plateau revealed by mass-balance model. *J. Glaciol.* **46**, 244–252 (2000). doi:10.3189/172756500781832945

61. A. Sakai, T. Nuimura, K. Fujita, S. Takenaka, H. Nagai, D. Lamsal, Climate regime of Asian glaciers revealed by GAMDAM glacier inventory. *Cryosphere* **9**, 865–880 (2015). doi:10.5194/tc-9-865-2015

62. A. Sakai, K. Fujita, Contrasting glacier responses to recent climate change in high-mountain Asia. *Sci. Rep.* **7**, 13717 (2017). doi:10.1038/s41598-017-14256-5 Medline

63. H. Zekollari, M. Huss, D. Farinotti, Modelling the future evolution of glaciers in the European Alps under the EURO-CORDEX RCM ensemble. *Cryosphere* **13**, 1125–1146 (2019). doi:10.5194/tc-13-1125-2019

64. L. Compagno, M. Huss, E. S. Miles, M. J. McCarthy, H. Zekollari, A. Dehecq, F. Pellicciotti, D. Farinotti, Modelling supraglacial debris-cover evolution from the single-glacier to the regional scale: An application to High Mountain Asia. *Cryosphere* **16**, 1697–1718 (2022). doi:10.5194/tc-16-1697-2022

65. R. H. Giesen, J. Oerlemans, Calibration of a surface mass balance model for global-scale applications. *Cryosphere* **6**, 1463–1481 (2012). doi:10.5194/tc-6-1463-2012

66. F. Maussion, F. Maussion, T. Rothenpieler, M. Dusch, P. Schmitt, A. Vlug, L. Schuster, N. Champollion, F. Li, B. Marzeion, M. Oberrauch, J. Eis, J. Landmann, A. Jarosch, A. Fischer, S. Hanus, D. Rounce, M. Castellani, S. L. Bartholomew, S. Minallah, C. Merrill, D. Otto, D. Loibl, L. Ultee, S. Thompson, P. Gregor, OGGM/oggm: v1.6.0, version v1.6.0, Zenodo (2023); https://doi.org/10.5281/zenodo.7718476.